Measurements, at Mach Numbers up to 2·8, of the Longitudinal Characteristics of One Plane and Three Cambered Slender 'Ogee' Wings

By C. R. Taylor

Communicated by the Deputy Controller Aircraft (Research and Development), Ministry of Aviation

*Reports and Memoranda No. 3328**
December, 1961

Summary.

Measurements have been made of the longitudinal characteristics of one plane and three cambered slender ogee wings ($p = 0{\cdot}45$, $s_T/c_0 = 0{\cdot}208$) at two subsonic and eight supersonic Mach numbers up to 2·8. The tests also included measurements of the zero-lift pressure drag and support interference of the plane wing. The results have been analysed to give data for estimating the performance of supersonic transport aircraft.

LIST OF CONTENTS

* Replaces R.A.E. Report No. Aero. 2658—A.R.C. 23,776.

LIST OF ILLUSTRATIONS

Figure

Approved For Release 2002/10/16 : CIA-RDP71B00822R000100080002-8

LIST OF ILLUSTRATIONS—*continued*

1. *Introduction.*

The purpose of this report is to describe tests, in the 8 ft × 8 ft Tunnel at Bedford, on four slender ogee wings. All four wings had the same planform ($p = 0{\cdot}45$, $s_T/c_0 = 0{\cdot}208$); one was plane and three were cambered to give varying amounts of centre-of-pressure shift at supersonic speeds. Measurements of lift, drag and pitching moment were made at two subsonic and eight supersonic speeds up to $M = 2{\cdot}8$ and the tests also included pressure measurements to determine the zero-lift pressure drag and support interference for the plane wing at supersonic speeds.

The present tests contribute to an extensive investigation of the aerodynamics of slender shapes and their suitability for long-range supersonic transport aircraft. As a result of earlier work in this investigation it has been suggested that it should be possible to design an aircraft having an acceptable performance and flight characteristics, utilizing wing flows which are both computable and physically realizable, provided that: (*a*) its planform is slender with streamwise tips (at all flight speeds the leading edges are 'subsonic') and the trailing edge is either straight or only slightly swept; (*b*) it is integrated, in the sense that the wing and body are smoothly blended together to form a single smooth wing-like shape, capable of lifting over its entire length; and (*c*) the leading edges are sharp and if the wing is cambered (in order to bring the centre of lift at cruising conditions near the position of the aerodynamic centre at low speeds), the camber loading is zero at the leading edges, so that the leading edges are attachment lines at the design incidence and at other incidences the flow separations are either wholly above or wholly below the wing[1, 2, 3]. A fundamental feature of the flow past these wings is that at all flight conditions there is primary separation from all edges and, under cruising conditions, the wing surface is free from shock waves. It should be noted that the

aerodynamic design point is not normally a flight condition. This is because, for wings with sharp and highly swept leading edges, the existing methods of design are only valid when the leading edges are attachment lines and it has been found that lower cruising drags are obtained by using design lift coefficients lower than the cruise value.

Earlier work in the slender-wing programme concentrated on wings of simple shape (e.g. wings with rhombic transverse cross-sections, having planforms and centre-line sections defined by simple polynomials), and the principal object of the tests described here, was to determine to what extent changes towards what was considered to be a more realistic shape would affect the high-speed drag and the ability of a simply designed camber to trim the wing. Thus, although the present wings conform to the restrictions of the preceding paragraph, considerations of an aircraft's stowage, balance and structural requirements have influenced the choice of planform and thickness distribution. Consequently, they have much of their volume concentrated near the centre-line and, compared with most of the earlier wings, the position of maximum cross-sectional area is farther aft, the mean trailing-edge angle and the minimum leading-edge angle are greater, and the planform parameter, $p \equiv \bar{c}/c_0$, has been reduced by 'waisting' the planform. For these wings the cruise condition is assumed to be $C_L = 0{\cdot}075$, $M = 2{\cdot}2$.

2. *Description of the Models.*

Four shapes were tested, one plane, the others cambered; all four had the same planform and thickness distribution.

The planform, which is defined by the equation

$$\frac{s(x)}{s_T} = \frac{x}{c_0}\left\{1{\cdot}2 - 2{\cdot}4\frac{x}{c_0} + 2{\cdot}2\frac{x^2}{c_0^2} + 3\frac{x^3}{c_0^3} - 3\frac{x^4}{c_0^4}\right\}$$

$$\frac{s_T}{c_0} = 0{\cdot}208,$$

is shown in Fig. 1, where it is compared with two gothic wings and two other ogee wings of the same slenderness parameter (s_T/c_0). It will be seen that the lower p-value for the present shape has been obtained by waisting the planform while maintaining an apex angle comparable with that of the gothic wing with $p = 7/12$. This has resulted in a shape having two points of inflexion and an uneven variation of leading-edge sweepback across the span (*see* Fig. 2).

The thickness distribution (Figs. 3, 4 and 5) is a 'lofted' shape without a defining equation. It is an example of how a smooth integrated fairing could enclose a realistic pressure cabin and outboard fuel tanks. For these wings it was proposed that the engines should be enclosed in under-wing boxes whose shapes followed those of the clean-aircraft streamlines. The streamwise variation of cross-sectional area is less smooth than those of earlier wings, the position of maximum area is farther back, and both the slope and curvature at the trailing edge are larger (*see* Fig 6).

The camber surfaces for these wings were designed by the slender-wing-theory method of Ref. 4*. Inboard of the 'shoulder lines' the streamwise slope of the mean surface is constant along the span but outboard of the shoulders it varies parabolically with the spanwise co-ordinate. The

* A computing programme for calculating the camber shape by linearized thin-wing theory was not available at the time. Slender-wing theory was chosen in preference to not-so-slender theory[17, 21, 22] because of its simplicity.

ratio between the values of the slope at the leading edge and at the centre is chosen such that the load vanishes at the leading edge. The ordinates of the mean surfaces have been obtained by integrating the surface slopes from a straight hinge-line at 95% root chord. The equation of the shoulder position is

$$\eta_0(x) = 0{\cdot}5 \qquad 0 \leqslant x \leqslant \frac{c_0}{2}$$

$$= 0{\cdot}5 + \left(\frac{x}{c_0} - \frac{1}{2}\right)^2 \qquad \frac{c_0}{2} \leqslant x \leqslant c_0$$

The shoulder position was chosen to be well inboard near the apex in order to avoid large adverse pressure gradients; it was chosen to be farther outboard near the trailing edge to obtain a low vortex drag[4]. The wings were cambered to give the following lift and pitching-moment coefficients:

Wing	C_{Ld}	C_{md}	α_d	θ	ΔC_m
15 (plane wing)	0	0	0	0	0
16	0	0·00853	0	30°	0·00853
17	0·025	0·00800	1°	50°	0·00853
18	0·025	0·00435	1°	40°	0·00487

The design incidence α_d is the inclination of the central part of the mean surface at the trailing edge ($\alpha = 0$ corresponds to the no-lift attitude according to slender-wing theory). The values of θ quoted are the maximum angles of leading-edge droop. At a lift coefficient of 0·075 the cambered wings are intended to have their centres of lift either 4% c_0 (wing 18) or 7% c_0 (wings 16 and 18) forward of that of the plane wing.

In order to be able to use slender-wing (i.e. $M = 1$) theory to design a camber surface to give a prescribed shift of centre of pressure at a cruise Mach number of 2·2, it has been assumed that, even though the centre-of-pressure positions of the wings may change with Mach number, the difference in C_m between the plane and cambered wings, at the cruise C_L, will not change and will be equal to the difference at the design lift coefficient. To decide the centre-of-pressure movement needed, it was also assumed that the aerodynamic centre at low speeds would not be affected by wing camber. With these assumptions it was expected that the ΔC_m required for this planform at $C_L = 0{\cdot}075$ would fall between the two values chosen (i.e. between 0·00487 and 0·00853). Details of the camber loadings and the shapes of the cambered wings are shown in Figs. 7, 8 and 9.

Except for the nose sections, wings 15 and 16 were machined from steel, whereas wings 17 and 18 were fabricated from glass-cloth bonded with Araldite. For the force tests the models were supported by a sting of 2·1 in. diameter and included a six-component strain-gauge balance (Fig. 10). On all the models the cylindrical sting shroud was symmetrically disposed at the trailing edge. An additional model of wing 15 was used for the pressure measurements; this was connected to a cranked sting by a thin yoke near the trailing edge (Fig. 10), which was designed to leave the upper surface of the wing free from support influence for $M \geqslant 1{\cdot}4$. The pressure holes (100 in number) were distributed along five chordwise stations, located so that they represented equal amounts of frontal area, i.e. at $y/s_T = 0{\cdot}032$, 0·096, 0·176, 0·336 and 0·656. A dummy sting shroud was available for the tests to investigate the shroud effect on zero-lift drag.

Table 1 lists all the model dimensions.

3. *Details of the Tests.*

In the force tests, measurements of normal force, pitching moment and axial force were made at Mach numbers 0·3 (approximately), 0·8 (approximately) and 1·4 (0·2) 2·8, at a constant Reynolds number of 10^7, based on root chord. The incidence range used was:

$$\alpha = -6°(1°)0(\tfrac{1}{2}°)6°(1°)12°$$

except at $M \simeq 0·3$ where

$$\alpha = -6°(1°)20°.$$

The models were tested both right-way-up and inverted in order to isolate the effects of flow deflections in the airstream (all the graphs in this Report refer to the mean of right-way-up and model-inverted results). All force coefficients are based on the plan area of the wings; the reference length for C_m is $\bar{c}$ (the second mean chord) and the moment reference point is at $0·5\bar{c}$, i.e. at the centre of the plan area.

The pressure measurements on wing 15 were made at $M = 1·4$, 1·8, 2·2 and 2·6 only; the Reynolds number again being 10^7, with an additional test at $M = 2·2$, $R = 1·5 \times 10^7$. The incidences tested were $\alpha = -2°(\tfrac{1}{2}°)2°$ and $\alpha = 0$ model inverted. The tests with the dummy shroud fitted were done only at zero incidence.

At $M = 2·0$ additional force measurements were made at Reynolds numbers of 5 and 15 millions, and the results were used to estimate the effects of model distortion under load. The results for the metal models showed no change with dynamic pressure (apart from the expected shift in the level of the drag polars), whereas for models 17 and 18 there were measurable changes in pitching moment and lift. The distortion corrections, at $M = 2·0$, for $R = 10^7$ were found to be: $\Delta\alpha/C_L = -1·5°$, $\Delta C_m/C_L = -0·010$; these corrections have been applied to the results for all supersonic Mach numbers.

The drag results in Figs. 13, 16, 21 and 22 are not corrected for the presence of the sting shroud, except that the axial force has been corrected to free-stream static pressure at the shroud base. The correction to the zero-lift drag of the plane wing has been derived from the pressure measurements, it is closely approximated by $\Delta C_{D0} = 0·00088 - 0·00053 \log \beta$ and is taken into account in the analysis of the zero-lift drag measurements on wing 15 in Section 4.3. On the cambered wings, except at the trailing edges, the sting shroud protruded from the upper and lower surfaces by different amounts, in effect distorting the camber surface. The estimated corrections for this are (*see* Appendix I for details):

Wing 16	$\Delta C_m = 0·0003/\beta$
17	$0·0008/\beta$
18	$0·0005/\beta$

these are included in all the plotted results for supersonic speeds.

The following tunnel-constraint corrections were applied to the results for subsonic speeds:

	$M \simeq 0·3$	$M \simeq 0·8$
$\Delta\alpha/C_L$	0·72°	0·82°
$\Delta C_m\alpha/C_L^2$	0·056	0·093
$\Delta C_D/C_L^2$	0·010	0·010

where α is measured from the no-lift attitude. These figures were derived by applying the method of Ref. 5 to this planform. The small blockage effect of these wings was allowed for by correcting the values of p_0 and $\frac{1}{2}\rho U^2$ given to the computer.

Estimates of the accuracy of the tests suggest that the errors in the plotted results are within the following limits:

$$C_L : \pm 0{\cdot}001 \quad \pm 0{\cdot}01 C_L$$
$$C_m : \pm 0{\cdot}0002 \pm 0{\cdot}01 C_m$$
$$C_D : \pm 0{\cdot}0003 + 0{\cdot}008 C_L^2$$

except for $M \simeq 0{\cdot}3$, where, due to the low dynamic pressure, the errors may be three times these values. For the pressure coefficients the random scatter, due to errors in pressure measurement, is thought to be less than $0{\cdot}004$; an additional error, due to uncertainty in the measurement of the true static pressure in the tunnel, is probably about $\pm 0{\cdot}005$ (this would affect all the readings at one Mach number by the same amount and would not affect the measured pressure drag). An additional error in pitching moment may arise from the unaccounted-for variation with Mach number of the distortion correction.

To promote boundary-layer transition near the leading edges, bands of 60 grade carborundum in Araldite were applied to the wings; these were $\frac{1}{2}$ in. wide and were located $\frac{1}{10}$ in. from the leading edges. This size of roughness (approximately $0{\cdot}010$ in.) was that required to cause transition at $M = 2{\cdot}8$; it is estimated that at $M = 1{\cdot}4$ it is $1{\cdot}7$ times, and at $M = 0{\cdot}3$ twice, the size needed. It did not cause transition at $M = 2{\cdot}0$, $R = 5 \times 10^6$.

Further measurements of the zero-lift drag of wing 15 were made while this report was being prepared, using a more sensitive balance which has recently become available. The conditions for these tests were:

(*a*) $R = 10^7$, $M = 1{\cdot}4$, $1{\cdot}8$, $2{\cdot}2$, $2{\cdot}4$, $2{\cdot}6$, and

(*b*) $R = 1{\cdot}5 \times 10^7$, $M = 1{\cdot}4$ ($0{\cdot}2$) $2{\cdot}2$.

The errors in C_D for these tests are thought to be less than $0{\cdot}0002$.

4. *Presentation and Discussion of the Results.*

4.1. *Introductory Remarks.*

The results of the force measurements at subsonic speeds are plotted in Figs. 11 to 16; Figs. 17 to 22 contain a selection of the force results for supersonic speeds and Figs. 27 and 28 show the measured pressure distributions for the plane wing.

In the analysis of wind-tunnel results for performance estimation it is current practice to divide the drag of the aircraft into three separate, and additive, components, viz.

$$C_D = C_{DF} + C_{D0W} + C_{DL} \tag{1}$$

of which only one, the skin-friction drag C_{DF}, is sensitive to changes in Reynolds number*. Of the remaining terms, C_{D0W} is the wave drag due to thickness and C_{DL} is the drag increment due to lift.

For the present series of tests, C_{D0W} is the zero-lift wave drag as measured on the plane wing and if this is expressed as

$$C_{D0W} = \frac{128}{\pi} \frac{V^2}{Sc_0^4} K_0, \tag{2}$$

then K_0 is the ratio of the zero-lift wave drag of a wing to that of the minimum-drag body of revolution having the same length and volume. No distinction is made between zero-lift wave drag and zero-lift pressure drag.

* The Reynolds number, based on length, for the full-scale aircraft at cruise is approximately $3{\cdot}5 \times 10^8$.

The lift-dependent drag, C_{DL}, may be expressed in the forms*:

$$C_{DL} = \frac{K}{\pi A} C_L^2 \tag{3}$$

$$= \frac{C_L^2}{\pi A}\left(K_r + 2\beta^2 \frac{s_T^2}{c_0^2} K_w\right), \tag{4}$$

where, in theory, $K_r = 1$ for an elliptic spanwise distribution of lift and $K_w = 1$ in the approximation of not-so-slender-wing theory for slender wings having an elliptic streamwise distribution of lift. The values of C_{DL} for $K_r = 1 = K_w$ are sometimes known as R. T. Jones's lower bound for the drag due to lift [1, 2, 6]. In general, K_r and K_w will vary with Mach number and lift coefficient.

In the following sections we consider first the subsonic characteristics of the wings, then the breakdown of the drag, according to equation (1), and finally the lift and pitching-moment characteristics.

4.2. *Results for Subsonic Speeds.*

In this section we consider those aspects of the results for subsonic speeds which are relevant to the performance of the aircraft, particularly those which affect the interpretation of the results for supersonic speeds. It should be noted that, for these wings: (*a*) the incidence corresponding to the landing-approach condition is about 14° and (*b*) the lift coefficient for 'hold' or 'diversion' at high subsonic speeds is approximately 0·10.

The lift vs. incidence plots for $M \simeq 0{\cdot}3$ and $M \simeq 0{\cdot}8$ (Figs. 11 and 14) show an increase in lift-curve slope with incidence as is usual for slender wings, the curves for all four wings being virtually parallel in the region of interest. The 'approach' incidence can be seen to correspond to a lift coefficient of approximately 0·45. At $M \simeq 0{\cdot}3$ the lift curve of the plane wing is closely approximated by $C_L/\alpha = 1{\cdot}21\{1 + 1{\cdot}45\alpha^{2/3}\}$, where α is in radians, a similar, but larger, variation of lift with incidence is given by the slender-wing theories of Adams and Edwards (cf. Ref. 7). The measured lift is approximately 7% more than that given by Peckham's generalised curve for flat-plate delta and gothic wings[9], if a small allowance for Mach number is made by replacing C_L by $\beta'^2 C_L$, α by $\beta'\alpha$ and s_T/c_0 by $\beta' s_T/c_0$; $\beta' = \sqrt{(1-M^2)}$.

An important feature of the results for $M \simeq 0{\cdot}3$ is the severe pitch-up (Figs. 12 and 23). For the plane wing the aerodynamic-centre position moves forward about 4% $\bar{c}$ with an increase in C_L from zero to the approach value; the movements are greater for the cambered wings and increase with increasing amounts of leading-edge droop. The aerodynamic centre of the non-linear lift on the plane wing has been estimated by assuming that the aerodynamic centre of the linear lift remains fixed at $0{\cdot}5\bar{c}$, its position at $C_L = 0$, and the linear and non-linear lift components are given by $1{\cdot}21\alpha$ (rad) and $1{\cdot}76\alpha^{5/3}$(rad) respectively. This shows, Fig. 24, that the aerodynamic centre of the non-linear lift is always ahead of that of the linear lift and moves forward rapidly with increasing lift coefficient. At $M \simeq 0{\cdot}8$, camber again has a destabilizing effect, but the pitch-up is less than at $M \simeq 0{\cdot}3$ and only occurs at lift coefficients greater than the flight value.

At both subsonic Mach numbers camber has little effect on drag due to lift; at $M \simeq 0{\cdot}3$ the cambered wings have slightly more drag than the plane wing, at $M \simeq 0{\cdot}8$ slightly less. At $M \simeq 0{\cdot}8$, the drag polar for the plane wing is a parabola with $K_r = 1{\cdot}54$. The cambered wings have vortex drag factors, at $C_L = 0{\cdot}1$, based on the C_{D0} of the plane wing, of 1·44 (wings 16 and 18) or 1·36 (wing 17).

* Throughout the analysis C_{DL} is the difference between C_D of the cambered wing and C_{D0} of the plane wing.

4.3. *Zero-Lift Drag of the Plane Wing.*

In this section we consider the first two terms in the drag breakdown {equation (1)}, i.e. we consider the division of the zero-lift drag of the plane wing into the skin-friction and pressure-drag components. The pressure tests on the plane wing were specifically designed to facilitate this analysis by providing measurements of the effects of the sting shroud and a direct measurement of the zero-lift pressure drag. A comparison of the measured pressure distributions with those given by slender-wing theory and linearised thin-wing theory was also intended.

Earlier tests in the slender-wing programme, mainly those on delta wings with rhombic cross sections and Newby or Lord V area distributions (cf. Fig. 6), have shown that the friction drag of these wings can be accurately estimated by calculating the drag of a flat plate of the same planform, assuming the boundary layer is locally two-dimensional, and multiplying this value by the ratio of the wetted area of the model to that of the flat plate. This method of estimating the skin friction has also been used here. The pressure drags of these earlier models are in close agreement with both linear-theory and slender-body-theory estimates of wave drag at low values of $\beta s_T/c_0$, where the results from the two theories agree; but at higher values of the slenderness parameter, where the theoretical values diverge, the experimental drags followed the lower (i.e. slender-body) estimate.

The breakdown of the zero-lift drag of wing 15 is shown in Fig. 25. The measured total-drag coefficients are increased by the correction for the masking effect and pressure field of the sting shroud. The difference between this corrected C_{D0} and the estimated friction-drag coefficient should be equal to the measured pressure drag but it is, in fact, 0·0003 to 0·0006 higher. The errors in the various measurements are thought to be within the following ranges:

C_{D0}	$\pm$ 0·0003 ($\pm$ 0·0002 for later tests)
Shroud correction	$\pm$ 0·0001
Pressure drag	$\pm$ 0·0001

so that the most adverse combination of these errors cannot entirely account for the discrepancies. It must be concluded therefore, that the friction drag is at least 5% higher than estimated.*

A comparison of the measured pressure drag with slender-body theory[9]† and linearized thin-wing theory[10]† estimates of the wave drag, Fig. 26, shows good agreement with linearized theory at all Mach numbers, and poor agreement with slender-body theory, thus reversing the trend of earlier results. However, the general level of K_0 is higher than that for wings with Newby or Lord V area distributions. It should be noted that, for wing 15, the difference between linearized and slender-body theories at the higher values of $\beta s_T/c_0$ is much larger than for Newby and Lord V area distributions and that Weber[11] has shown that differences of this order are typical of wings with comparably large values of $-c_0^2 S'(x)/V$ and $-c_0^3 S''(x)/V$ at the trailing edge. For these locally 'non-slender' wings one must expect the zero-lift wave drag to be much closer to the linearized-theory value than to the slender-body-theory value. Recent calculations of the zero-lift wave drag of a family of delta wings with rhombic cross-sections[12], using linearized theory, have shown that, even for the

* In the light of more recent tests this conclusion should be modified. It now appears that the friction drag is no greater than was estimated. The discrepancies noted are due to the drag of the bands of carborundum grit used to fix transition (cf. Appendix II).

† See Acknowledgements.

'optimum'* wings, the values of K_0 increase when the position of maximum cross-sectional area is moved aft beyond $0{\cdot}65c_0$. Thus, it can be expected that the relatively high drag of wing 15 is mainly due to the relatively rearward position of the maximum cross-sectional area (*see* Fig. 6), which is partly a result of the low p-value of the planform.

Further confirmation of the accuracy of linearized theory[13] is given by the excellent agreement of the theoretical pressure distribution with the measured values for $M = 2{\cdot}2$, shown in Fig. 27. The agreement here appears to be much better than, for example, that normally found between pressure distributions in two-dimensional flow over aerofoil sections at low speeds and the corresponding linearized approximations. By comparison, the slender-thin-wing-theory[13] estimate, while giving reasonable accuracy over the front of the wing, is seriously in error over the rear $25\%\ c_0$, where the shape becomes non-slender. It should be noticed that the measured pressure coefficients are quite small (Figs. 27 and 28) and therefore an important assumption in linearized theory, viz. that the perturbations are small, is genuinely satisfied.

4.4. *Drag-due-to-Lift at Supersonic Speeds.*

We turn now to the last term in the drag breakdown and consider the lift-dependent drag of all four wings.

In the absence of any theoretical method of estimating the lift-dependent drag for wings with leading-edge separation we rely entirely on wind-tunnel measurements and their analysis in terms of simple geometric parameters. Such an analysis of early measurements of the lift-dependent drag of plane slender wings has been made by Courtney[14]. He found that if he plotted $K = \pi A(C_D - C_{D0})/C_L^2$, for $C_L = 0{\cdot}1$, against βA, all the points for sharp-edged plane wings with streamwise tips lay close to the line

$$K = 0{\cdot}75 + 0{\cdot}64\beta A, \qquad 1{\cdot}2 \leqslant \beta A \leqslant 3{\cdot}2.$$

These values of K, and also those for sharp-edged delta wings, are, in general, lower than those for round-nosed delta wings collected and analysed by Cane and Collingbourne some years earlier, implying that the loss of leading-edge thrust due to sharpening the leading edge is more than compensated by the resulting leading-edge flow separation, (*a*) increasing the lift for a given incidence and (*b*) producing higher over-wing suctions than under-wing pressures on the forward-facing surfaces near the leading edges. For camber distributions with attached flow at a C_L lower than the cruise C_L the high loadings near the leading edges act on the drooped parts of the wing, with the result that, although the minimum drag coefficient may be increased slightly, the curvature of the drag polar is reduced sufficiently to give a lower C_D, and hence K, at the cruising C_L (as in Figs. 21 and 22). Thus the values of K given by Courtney's curve form an upper limit to the range of values we would expect for cambered wings; a lower limit is given by R. T. Jones's lower bound[1, 2, 6] although this is no real physical limit and lower values may, in principle, be obtainable.

The values of K derived from a comparison of the drags of the cambered wings *with the zero-lift drag of the plane wing* are shown in Fig. 29. It should be noted that although the potential errors in these plots are quite large (e.g. $\Delta K = \pm 0{\cdot}045 \pm 0{\cdot}0018/C_L^2$ for the worst combination of the errors listed in Section 3) the actual uncertainty in the points plotted is thought to be no more than the

* The 'optimum' wings are those members of the family having the smallest drag for a fixed position of the maximum cross-sectional area, at a given $\beta s_T/c_0$.

scatter about the mean lines shown on the figures. For all the wings the variation of K with Mach number is of the form $K = K_r + 2K_w\beta^2 s_T^2/c_0^2$ with the following values for K_r and K_w:

Wing	$C_L = 0{\cdot}075$		$C_L = 0{\cdot}100$		$C_L = 0{\cdot}125$	
	K_r	K_w	K_r	K_w	K_r	K_w
15	1·28	2·10	1·44	1·94	1·48	1·94
16	1·33	1·70	1·39	1·57	1·41	1·64
17	1·18	2·04	1·22	1·76	1·22	1·78
18	1·23	1·74	1·22	1·76	1·30	1·56

All the cambered wings have lower values of K_r and K_w, and hence lower values of K, than the plane wing. For the range of leading-edge droop angle covered by the cambered wings (i.e. 30° to 50°) an increase in droop decreases K_r, increases K_w and, in general, decreases K. For $C_L = 0{\cdot}10$ it is only the more highly cambered wings which have values of K lower than those of Courtney's curve. The drag factors for the plane wing are at least 0·15 higher than his values but, nevertheless, they are still 0·25 lower than the value for zero axial force (i.e. $\pi A\alpha/C_L$ in Fig. 30), which is better than average for wings of this $V/S\bar{c}$*, implying that the main reason for the high lift-dependent drag of this family of wings is the low lift-curve slope of the planform. This is a direct consequence of the low value of p; as is shown in Fig. 31, where values of $\pi A\alpha/C_L$ for $C_L = 0{\cdot}1$, obtained from recent tests on plane gothic and ogee wings[15, 16, 17, 18], are compared with the value for wing 15 at the same $\beta s_T/c_0$ and the same βA.

4.5. *Lift and Pitching Moment at Supersonic Speeds.*

In this section we discuss the supersonic lift and pitching-moment characteristics and assess the effectiveness of the camber designs as means of trimming the wings at the cruise condition. In the previous section it was shown that for lift coefficients greater than about 0·07 the cambered wings have lower drags than the plane wing. It is also known that conventional trailing-edge controls may be very inefficient trimming devices (e.g. wind-tunnel tests of a model of the F.D.2 delta-wing research aircraft[19] have shown that, at supersonic speeds, the lift-dependent drag factor of the trimmed configuration is twice that for the fixed-elevator cases). Thus there is a considerable incentive to trim a supersonic aircraft, at cruising conditions, using camber alone.

A comparison of the lift vs. incidence curves of the four wings shows that the cambers tested had no significant effect on the development of lift with departures from the design incidence (to make this comparison in Figs. 17 and 18 the curves for wings 17 and 18 should be displaced 1° to the left). Similarly, if allowance is made for the possible errors in the distortion corrections for wings 17 and 18, it is found that the camber has very little effect on the aerodynamic-centre position at supersonic speeds. The variations of $\partial C_L/\partial\alpha$ and $-\partial C_m/\partial C_L$ for the plane wing, shown in Figs. 32 and 33, therefore may be regarded as representative of all four wings. At all Mach numbers the lift vs. incidence curves become straight for $\beta(\alpha-\alpha_0)$ greater than about 3° and two values of $\partial C_L/\partial\alpha$ are plotted in Fig. 32. It is noticeable that, at the lower supersonic Mach numbers, where there is

* e.g. $(\pi A\alpha/C_L - K)_{C_L=0{\cdot}1}$ varies from 0·10 to 0·30 for the wings of Refs. 16 to 19.

more lift due to leading-edge separation, the C_m vs. C_L curves are quite straight, implying that the centres of linear and non-linear lift are virtually coincident. At the higher Mach numbers there is less non-linear lift but the aerodynamic-centre position moves forward with increasing C_L.

Figs. 32 and 33 also show values of these two derivatives given by two approximate theories, both of which assume that the flow remains attached at the leading edge. Not-so-slender-wing theory[20], which has given good agreement with linear theory for conical wings and reasonable agreement with experimental results for sharp-edged gothic wings[21], is clearly of limited use for the present planform, with its highly curved leading edge. On the other hand Evvard's approximate theory[22, 23], which was not expected to be of much use for this slender highly curved planform, appears to give a fair estimate of the lift-curve slope at zero incidence and a quite reasonable estimate of the aerodynamic-centre position at zero lift.

Turning to the trimming effectiveness of the wings, we recall that the cruising condition was assumed to be $C_L = 0{\cdot}075$ at $M = 2{\cdot}2$* and at this condition the wings should give centre-of-pressure shifts of either 4% c_0 (wing 18) or 7% c_0 (wings 16 and 17). Further, the low-speed results have shown that, at approach conditions, there is a progressive forward movement of the aerodynamic-centre position with increasing leading-edge droop. Thus in considering the trimming effectiveness of the camber we must take into account the fact that each wing will have a different most rearward c.g. position, dictated by the low-speed longitudinal stability requirements.

Reference to the C_m vs. C_L curves for $M = 2{\cdot}2$ in Fig. 20 shows immediately that none of the cambered wings achieves a satisfactory trimmed C_L. The values of ΔC_m (i.e. $C_m - (C_m)_{\text{wing 15}}$ at the same C_L) and the shift of the centre of pressure for $C_L = 0{\cdot}075$ actually obtained are shown in Fig. 34. It appears that, without allowing for the low-speed characteristics, wings 17 and 18 give about half the C.P. shift assumed and wing 16 about one third. However, when the pitching-moment reference points are moved forward to coincide with the low-speed aerodynamic-centre positions for $C_L = 0{\cdot}45$, as in Fig. 35, then, at $M = 2{\cdot}2$, the effective centre-of-pressure movements are only $1\frac{1}{2}\% c_0$ for wing 16, 2% c_0 for wing 17 and 1% c_0 for wing 18, when a shift of $5\frac{1}{2}\%$ c_0 is needed to trim.

Some indication of the manner in which the camber designs have failed to give their desired performance is given by the variation of lift and pitching moment with Mach number at design attitude (Fig. 36). These plots show that, if the design C_L and C_m are attained at $\beta s_T/c_0 = 0$, then there must be a very rapid increase in C_L at α_d with Mach number for $1 \leqslant M \leqslant 1{\cdot}4$, due, no doubt, to loss of the designed negative lift near the trailing edge (*see* Fig. 8)—wing 16, which calls for the largest amount of negative lift, being the most sensitive to changes in Mach number. Measurements of the load distribution on wing 17[24] confirm that for this wing the designed negative lift near the trailing edge is not achieved, even at $M = 1{\cdot}4$, and also show that, at low Mach numbers, the region near the apex develops considerably more than the design lift. The rearward movement of the centre of pressure with further increases in Mach number is due to increasing lift near the trailing edge and decreasing lift near the apex.

On any non-conical cambered wing one must expect a rearward movement of the centre of pressure of the camber loading with increasing Mach number above $M = 1$; one must also expect a rearward movement of the aerodynamic-centre position. Whether the changes in these two quantities follow one another in such a way that the value of C_{m0} remains constant must depend on

* Higher lift coefficients, of the order 0·10, are now being considered.

both the planform and the camber loading. Clearly, the planforms with higher values of p, with their larger chords near the tips, will have larger movements of aerodynamic-centre position (e.g. for a gothic wing, the change in x_{ac} in going from $M = 1$ to $M = 2$ is 12% c_0[15], compared with 3% c_0 for wing 15) and correspondingly larger changes in the centre-of-pressure position of the camber loading can be tolerated. The present wings failed to maintain their designed ΔC_m because the changes in the centres of pressure of the camber loadings outstripped the shift in aerodynamic centre (which was not as large as expected), mainly due, as we have seen, to the rapidly varying camber loadings near the trailing edge being too sensitive to changes in Mach number. A more-favourable result could be expected from wings with less-curved planforms and higher values of p, using smoother camber loadings. However, it may not be possible to utilize planforms and camber loadings which are smooth enough to justify the use of slender-wing theory and, in general, it would seem necessary to calculate the shape of the mean surface by linearized theory for the cruise Mach number.

5. *Conclusions.*

Analysis of the results to provide data for performance estimation, and comparisons with earlier results, has shown that:

(i) the zero-lift wave drag and zero-lift pressure distribution for the plane wing are both in close agreement with predictions of linearized thin-wing theory;

(ii) the zero-lift wave drag of the plane wing is higher than the values for wings of the same volume and length obtained in the earlier tests; this is attributed to the relatively rearward position of the maximum cross-sectional area, which partly results from the relatively low value of the planform shape parameter, $p \equiv \bar{c}/c_0$;

(iii) the lift-dependent drag factors of the wings are higher than those of other slender wings, when compared at the same value of βA; this is mainly due to the low lift-curve slope of the wings, which, in turn, is due to the low value of p;

(iv) the camber shapes designed by slender-wing theory do not give the desired changes in centre of pressure at $M = 2{\cdot}2$, the 'non-slender' camber loadings being more sensitive to changes in Mach number than the incidence loading;

(v) the trimming effectiveness of the cambered wings is significantly reduced by 'pitch-up' at the low-speed approach condition, the more-cambered wings being more affected.

An obvious implication of these conclusions is that a better aerodynamic performance would be obtained from a wing with a less-curved planform, having a higher value of p. Such a wing would be expected to have: (*a*) a more forward position of maximum cross-sectional area and therefore a lower zero-lift wave drag, (*b*) a higher lift-curve slope and therefore a lower lift-dependent drag, and (*c*) less pitch-up at low speeds. A better trimming effectiveness of the camber for such a wing would also be expected if a smoother camber loading were used and the mean surface were calculated by linearized theory.

6. *Acknowledgements.*

The author is indebted to Dr. J. Weber (R.A.E. Farnborough) for her calculation of the slender-body-theory and linear-theory wave drags for wing 15 (Fig. 26), to Mr. J. H. B. Smith (R.A.E. Farnborough) for the linear thin-wing-theory pressure distribution and to Dr. C. S. Sinnott (Hawker-Siddeley Aviation Limited) for the slender-thin-wing pressure distribution for wing 15 (Fig. 27).

LIST OF SYMBOLS

A		Aspect ratio, $4s_T^2/S$
$c(y)$		Local wing chord
c_0		Root chord
$\bar{c}$		First mean chord
$\bar{\bar{c}}$		Second (aerodynamic) mean chord
C_D		Drag coefficient
C_{D0}		Zero-lift drag coefficient of plane wing
C_{DL}		$C_D - C_{D0}$, where C_{D0} is zero-lift drag of plane wing
C_L		Lift coefficient
C_{Ld}		Design lift coefficient
C_m		Pitching-moment coefficient (based on $\bar{\bar{c}}$)
C_{md}		Design pitching-moment coefficient
C_p		Pressure coefficient
K		Lift-dependent drag factor (*see* Fig. 29)
$L(x)$		Spanwise integral of loading/$\frac{1}{2}\rho U^2$
M		Mach number of free stream
p		Planform parameter, $\bar{\bar{c}}/c_0$
R		Reynolds number based on c_0
$s(x)$		Local semi-span
s_T		Semi-span
S		Plan area
$S(x)$		Cross-sectional area (Fig. 6)
$t(y)$		Local maximum wing thickness
V		Wing volume
x, y, z		Cartesian co-ordinates with origin at wing apex
α		Incidence (in degrees unless stated otherwise)
α_d		Incidence at design attitude
β	$=$	$\sqrt{(M^2-1)}$
β'	$=$	$\sqrt{(1-M^2)}$
Λ		Angle of sweepback of leading edge
τ		Volume parameter, $V/S^{3/2}$
ΔC_m	$=$	$C_m - (C_m)_{\text{wing 15}}$, at constant C_L
$(\Delta C_m)_{\text{a.c.}}$	$=$	ΔC_m, referred to low-speed A.C. for $C_L = 0{\cdot}45$
ξ	$=$	$\{x + c(y) - c_0\}/c(y)$, non-dimensional chordwise co-ordinate
$\eta(x)$	$=$	$y/s(x)$

REFERENCES

No.	Author(s)	Title, etc.
1	D. Kuchemann	Aircraft shapes and their aerodynamics for flight at supersonic speeds. *Advances in Aeronautical Sciences*, Vol. 3, p. 221. Pergamon Press. 1961. Proc. 2nd int. congr. Aero. Sci., Zürich. 12 to 16 September, 1960.
2	E. C. Maskell and J. Weber ..	On the aerodynamic design of slender wings. *J. R. Ae. Soc.*, Vol. 63, No. 588, p. 709. December, 1959.
3	J. H. B. Smith	The problem of trim for a supersonic slender-wing aircraft. Unpublished M.o.A. Report.
4	J. Weber	Design of warped slender wings with the attachment line along the leading edge. A.R.C. 20,051. September, 1957.
5	S. B. Berndt	Wind-tunnel interference due to lift for delta wings of small aspect ratio. K.T.H. Aero. Tech. Note 19. Sweden. 1950.
6	R. T. Jones	The minimum drag of thin wings in frictionless flow. *J. Ae. Sci.*, Vol. 18, No. 2, p. 75. February, 1951.
7	J. Weber	Some effects of flow separation on slender delta wings. A.R.C. 18,073. November, 1955.
8	D. H. Peckham	Low-speed wind-tunnel tests on a series of uncambered slender pointed wings with sharp edges. A.R.C. R. & M. 3186. December, 1958.
9	M. J. Lighthill	The wave drag at zero lift of slender delta wings and similar configurations. *J. Fluid Mech.*, Vol. 1, Part 3, p. 337. September, 1956.
10	H. Lomax	The wave drag of arbitrary configurations in linearized flow, as determined by areas and forces in oblique planes. N.A.C.A. Research Memo. A55A18. March, 1955.
11	J. Weber	Some notes on the zero-lift wave drag of slender wings with unswept trailing edge. A.R.C. R. & M. 3222. December, 1959.
12	J. H. B. Smith and W. Thomson	The calculated effect of the station of maximum cross-sectional area on the wave drag of delta wings. A.R.C. C.P. 606. September, 1961.
13	J. Weber	Slender delta wings with sharp edges at zero lift. A.R.C. 19,549. May, 1957.
14	A. L. Courtney	A collection of data on the lift-dependent drag of uncambered slender wings at supersonic speeds. Unpublished M.o.A. Report.

REFERENCES—*continued*

No.	*Author(s)*	*Title, etc.*
15	L. C. Squire	An experimental investigation at supersonic speeds of the characteristics of two gothic wings, one plane and one cambered. A.R.C. R. & M. 3211. May, 1959.
16	L. C. Squire	The characteristics of some slender cambered wings at Mach numbers from 0·4 to 2·0. Unpublished M.o.A. Report.
17	D. G. Mabey and G. P. Ilott ..	The characteristics of three slender 'mild ogee' wings at Mach numbers from 0·4 to 2·0. Unpublished M.o.A. Report.
18	A. L. Courtney and A. O. Ormerod	Pressure plotting and force tests at Mach numbers up to 2·8 of an uncambered slender wing of $p = \frac{1}{2}$, $s_T/c_0 = \frac{1}{4}$ (Handley Page Ogee). A.R.C. 23,109. May, 1961.
19	C. R. Taylor and T. A. Cook ..	Six component force measurements on a 1/9th scale model of the Fairy Delta 2 research aircraft at Mach numbers up to 2·0. Unpublished M.o.A. Report.
20	MacC. Adams and W. R. Sears ..	Slender-body-theory review and extension. *J. Ae. Sci.*, Vol. 20, No. 2. August, 1959.
21	L. C. Squire	Some applications of 'not-so-slender' wing theory to wings with curved leading edges. A.R.C. R. & M. 3278. July, 1960.
22	J. C. Evvard	The effects of yawing thin pointed wings at supersonic speeds. N.A.C.A. Tech. Note 1429. September, 1947.
23	J. Gilbert	Approximate method for computing the pressure distribution on wings with subsonic leading edges in a steady stream. English Electric Aero. Tech. Memo. AM18. 1956.
24	J. Britton	Pressure measurements on a cambered ogee wing ($p = 0·45$) at Mach numbers up to 2·6. Unpublished M.o.A. Report.
25	W. R. Sears (editor)	*General theory of high speed aerodynamics.* (Vol. VI of *High Speed Aerodynamics and Jet Propulsion.*) Princeton University Press. 1955.
26	J. C. Evvard	Use of source distributions for evaluating theoretical aerodynamics of thin finite wings at supersonic speeds. N.A.C.A. Report 951. A.R.C. 13,821. 1950.
27	C. Kell	Free-flight measurements of the zero-lift drag of a slender wing at Mach numbers between 1·4 and 2·7. A.R.C. 23,511. August, 1961.
28	R. J. Monaghan	Formulae and approximations for aerodynamic heating rates in high speed flight. A.R.C. C.P. 360. October, 1955.
29	J. B. W. Edwards	Free-flight measurements of the zero-lift drag of a slender ogee wing at transonic and supersonic speeds. A.R.C. 24,448. October, 1962.

APPENDIX I

Corrections to Measured Lift and Pitching Moment for Asymmetry of the Sting Shroud

The asymmetry of the sting shroud distorts the mean surface. In the notation of Fig. 37 the distortion is

$$\Delta\bar{z}(x, y) = \tfrac{1}{2}\{\Delta z_U(x, y) - \Delta z_L(x, y)\} \tag{5}$$

and the corresponding additional incidence is

$$\Delta\alpha(x, y) = -\frac{\partial}{\partial x}\Delta\bar{z}(x, y). \tag{6}$$

To calculate the additional lift $\Delta\bar{L}(x)$ induced by the distortion on the segment of the wing between $x' = 0$ and $x' = x$ we utilize a flow-reversal theorem (cf. p. 235 of Ref. 25) which, for the present application, states that:

$$\Delta\bar{L}(x) = \int_0^x \int_{-r}^{r} \Delta\alpha(x', y') \frac{\Delta p(x', y': x)}{\alpha}\, dy'\, dx' \tag{7}$$

where $\Delta p(x', y': x)$ is the loading, at a point (x', y'), on a flat-plate wing, of the same planform as the wing segment $0 \leqslant x' \leqslant x$, at incidence α in reverse flow.

It follows from relations (5) and (6) that

$$\begin{aligned}\int_{-r}^{r} \Delta\alpha(x', y')dy' &= -\tfrac{1}{2}\frac{d}{dx'}\int_{-r}^{r}(\Delta z_4 - \Delta z_2)dy' \\ &= -\tfrac{1}{2}\frac{d\sigma(x')}{dx'}\end{aligned}$$

where $\sigma(x')$ is the difference between the additional cross-sectional areas on the upper and lower surfaces. We may approximate $\Delta p(x', y': x)$ in the region $0 \leqslant |y'| \leqslant r(x)$ by its value in the centre and thus obtain for $\Delta\bar{L}(x)$ the approximate value

$$\Delta\bar{L}(x) = -\tfrac{1}{2}\int_0^x \frac{d\sigma}{dx'}\frac{\Delta p(x', 0: x)}{\alpha}\, dx'. \tag{8}$$

The wing segments in reversed flow are wings with supersonic leading edges and subsonic trailing edges. If $x - x' \leqslant \beta s(x)$, then the loading is the same as in two-dimensional flow:

$$\frac{2}{\rho U^2}\frac{\Delta p}{\alpha} = \frac{4}{\beta}.$$

If $\beta s(x) \leqslant x - x' \leqslant \beta s(x) + 2\beta s(x_0)$, then the loading on the centre-line can be determined by Evvard's[26] method. The solution which satisfies the Kutta-Joukowski condition at the subsonic trailing edges reads:

$$\begin{aligned}\frac{2}{\rho U^2}\frac{\Delta p}{\alpha} &= \operatorname{sgn} y_1 \frac{8}{\pi}\int_0^{y_1}\{(x-x')^2 - \beta^2 y^2\}^{-1/2}dy \\ &= \frac{8}{\pi\beta}\sin^{-1}\frac{\beta y_1}{x - x'}.\end{aligned}$$

(87542)

When the upper- and lower-surface distortion fields do not interact, i.e. when $x < \beta s(x)$,

$$\frac{2}{\rho \bar{U}^2} \Delta \bar{L}(x) = -\frac{2}{\beta} \sigma(x)$$

and, since the loading $\Delta p/\alpha$ is constant over the entire area of the distortion, this expression is exact. In other cases y_1 must be found by geometrical construction and $\Delta \bar{L}(x)$ by integration.

The corrections to measured lift and pitching moment are:

$$\Delta C_L = -\frac{2}{\rho \bar{U}^2 S} \Delta \bar{L}(x_T)$$

and, for moment coefficients about $\bar{c}/2$, based on $\bar{c}$,

$$\Delta C_m = -\tfrac{1}{2} \Delta C_L - \frac{2}{\rho \bar{U}^2 S \bar{c}} \int_0^{x_T} \Delta \bar{L}(x) dx .$$

For wings 16 to 18, $x_T/s_T = 1{\cdot}5$ so that for $M \geqslant 1{\cdot}8$:

$$\Delta C_L = -\frac{2\sigma(x_T)}{\beta S} = 0$$

and

$$\Delta C_m = \frac{2}{\beta S \bar{c}} \int_0^{x_T} \sigma(x) dx$$

$$= 0{\cdot}0003/\beta \text{ for wing } 16$$

$$= 0{\cdot}0008/\beta \text{ for wing } 17$$

$$= 0{\cdot}0005/\beta \text{ for wing } 18 .$$

At $M = 1{\cdot}4$ and $1{\cdot}6$ the calculated differences from the above values were less than the probable experimental errors.

APPENDIX II

Kell's free-flight measurements of the zero-lift drag of the plane wing

In Ref. 27 Kell describes his free-flight measurements of the zero-lift drag of the plane wing (i.e. wing 15) between $M = 1{\cdot}4$ and $2{\cdot}7$. His results are reproduced in Fig. 38; also shown in this figure are his estimates of the drag of the small sting and stabilising fin (*see* Fig. 39) and the wing friction drag. The model was flown with transition fixing bands of $0{\cdot}007$ in. carborundum grit $0{\cdot}5$ in. wide, located $\frac{1}{10}$ in. from the leading edges. The turbulent-skin-friction drag was estimated using the intermediate-enthalpy methods of Ref. 28. Estimates of the probable heating rates of the model were based on the flight history and the known thermal properties of the model. In order to illustrate the significance of the heat-transfer rate, Kell estimated values of skin-friction drag assuming full and zero heat transfer; these are also plotted in Fig. 38. These last two estimates are only intended to illustrate the significance of the heat-transfer conditions, they are not intended to indicate the limits of accuracy of the skin-friction estimates.

The Reynolds number during the test varied from 42×10^6 at $M = 1{\cdot}4$ to 105×10^6 at $M = 2{\cdot}7$.

The comparison of the 'apparent wave drag' deduced from the free-flight results with that from the tunnel force measurements for $R = 10^7$ and with the tunnel measurements of pressure drag is shown in Fig. 40. The 'apparent wave drag' is the total measured drag less the sum of the estimated friction drag and the sting drag, and fin drag (if any). In the region of principal interest, i.e. near $M = 2{\cdot}2$, the free-flight results are about $0{\cdot}0005$ higher than the tunnel force results and $0{\cdot}0008$ higher than the measured pressure drag. It is now recognised that, in both the tunnel and flight tests, there were significant drag increments due to the roughness bands which were not taken into account in the analyses of zero-lift drag.* The roughness drag increment in the free-flight tests is expected to be larger than that for the tunnel tests since the grit used in flight was excessively coarse for the high Reynolds number of the tests. In view of the surprisingly large drag increments in the tunnel—$0{\cdot}0003$ at $R = 10^7$ and $0{\cdot}0005$ at $R = 1{\cdot}5 \times 10^7$ for a grit which did not provoke transition completely at $R = 0{\cdot}5 \times 10^7$—it could be anticipated that the drag of the transition trip accounts for, at least, a major part of the discrepancy between the apparent wave drag derived from the flight measurements and the tunnel measurement of pressure drag.

* See footnote in Section 4.3 and Section 4.5 of Ref. 29.

TABLE

Details of the Models

Length	(c_0)	60 in.
Span	($2s_{y'}$)	24·96 in.
Plan area	(S)	674 in.^{2}
Volume	(V)	726 in.^{3} (excluding sting shroud)
Surface area		1420 in.^{2} (including sting shroud)
Sting-shroud diameter		2·60 in.
Sting diameter		2·10 in.
Planform parameter (p)		0·45
Aspect ratio		0·924
$\bar{c}/c_0$		0·616
$\tau = V/S^{3/2}$		0·0415
$V/S\bar{c}$		0·040
$K_0/C_{D0} = \frac{\pi}{128} S \frac{c_0^4}{V^2}$		406·5

Moment reference point at $0{\cdot}5\bar{c}$ (i.e. at centre of plan area)

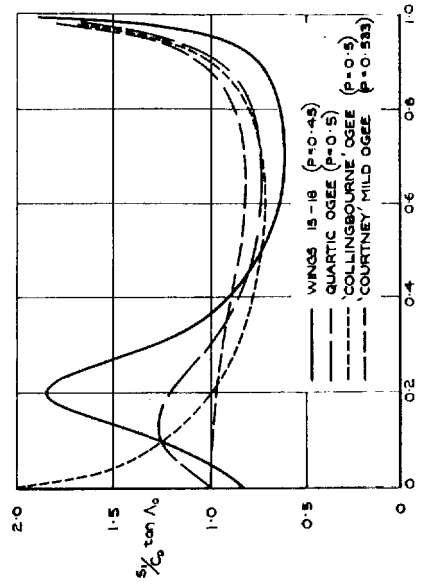

FIG. 2. Variation of leading-edge sweepback across the span.

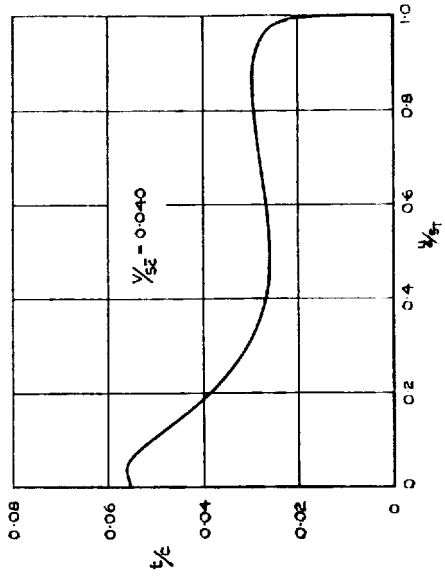

FIG. 3. Variation of thickness/chord ratio across the span.

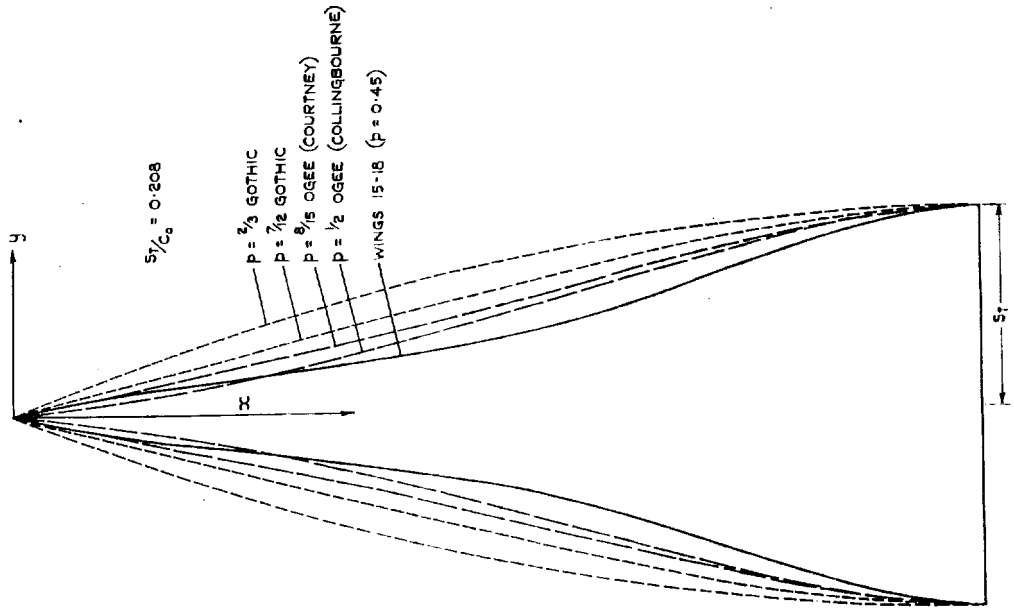

FIG. 1. The planform.

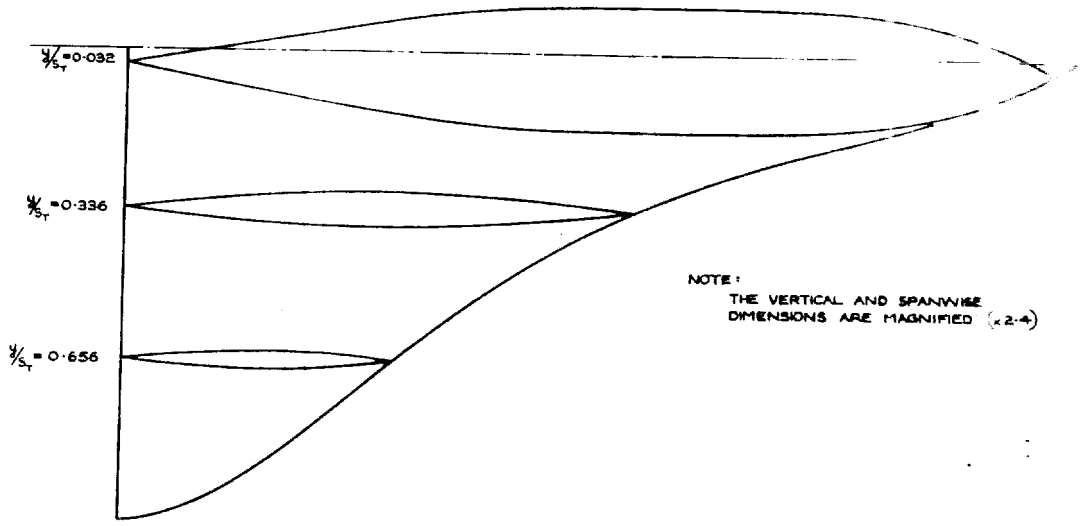

FIG. 4. The thickness distribution—chordwise sections.

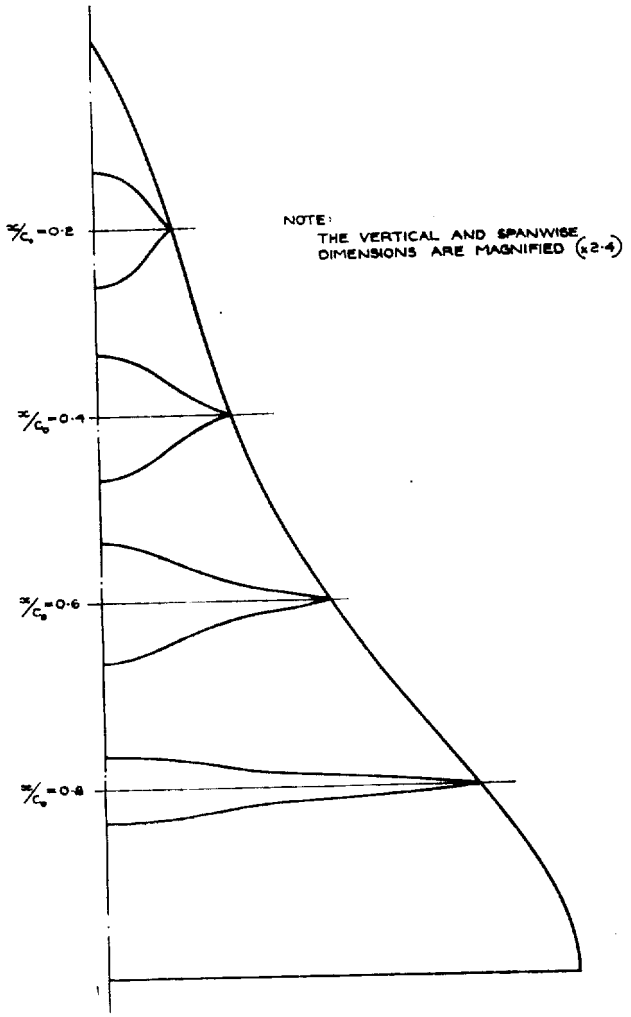

FIG. 5. The thickness distribution—spanwise sections.

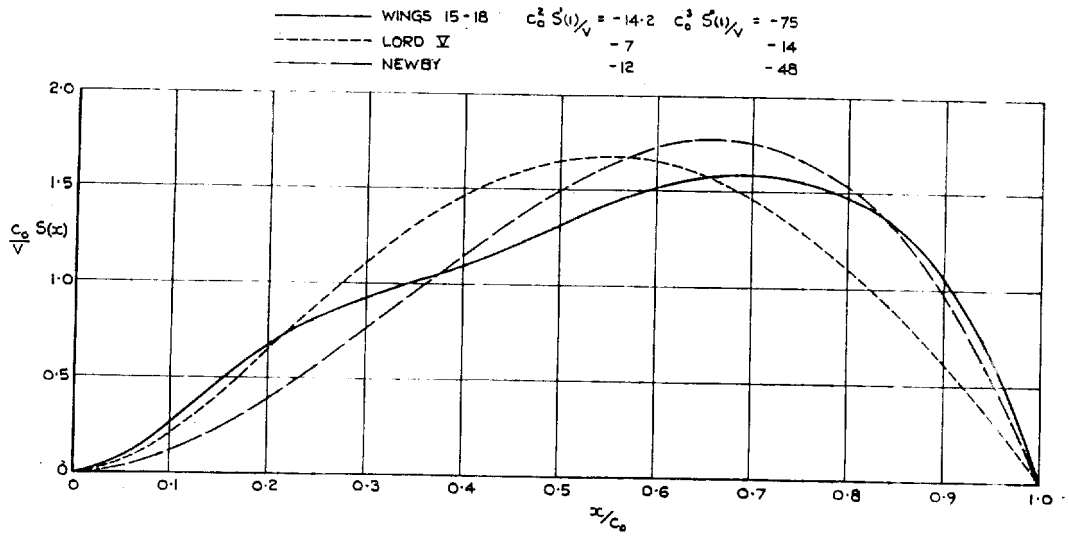

FIG. 6. Cross-sectional area distribution.

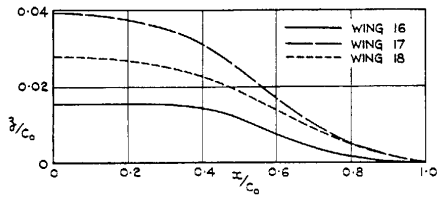

FIG. 7. Centre-line camber, wings 16, 17 and 18.

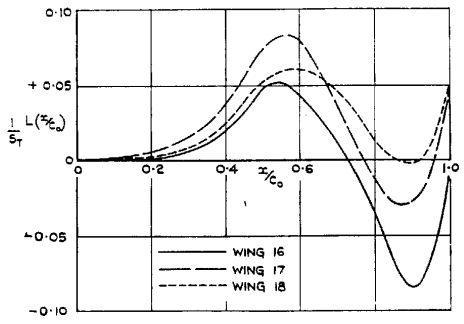

FIG. 8. Chordwise variation of camber loading for wings 16, 17 and 18, as assumed in slender-wing theory.

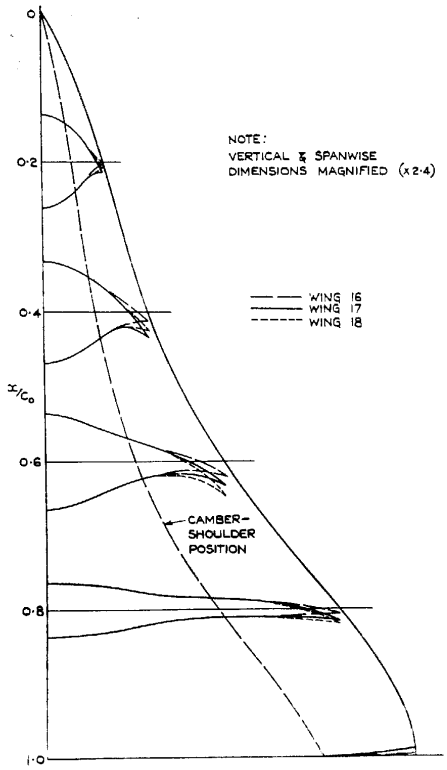

FIG. 9. Details of wings 16, 17 and 18.

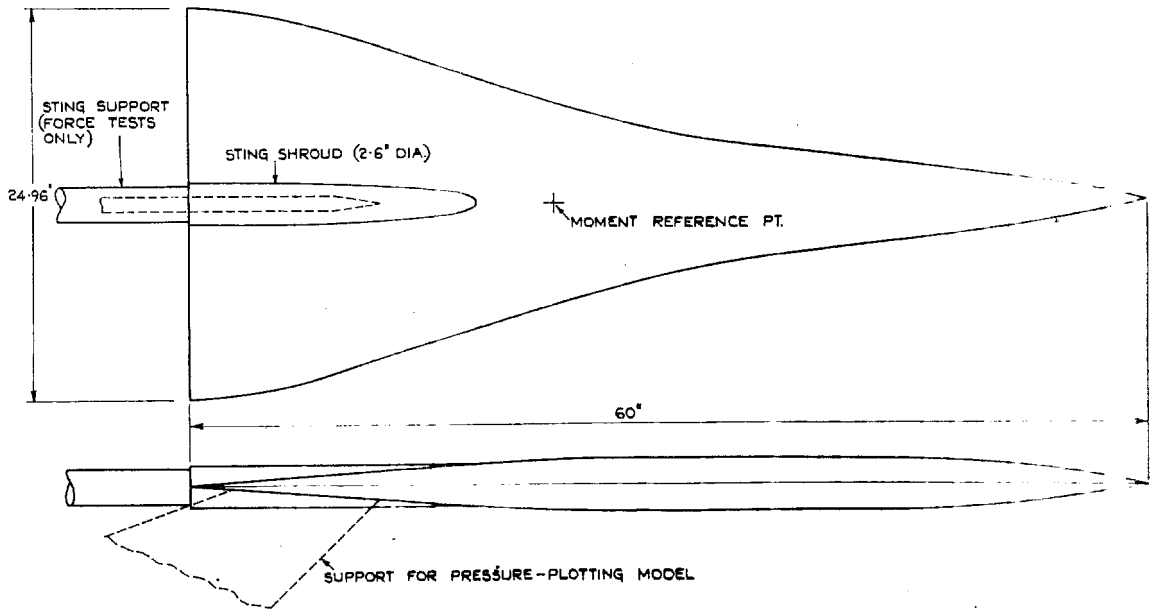

FIG. 10. Details of model supports.

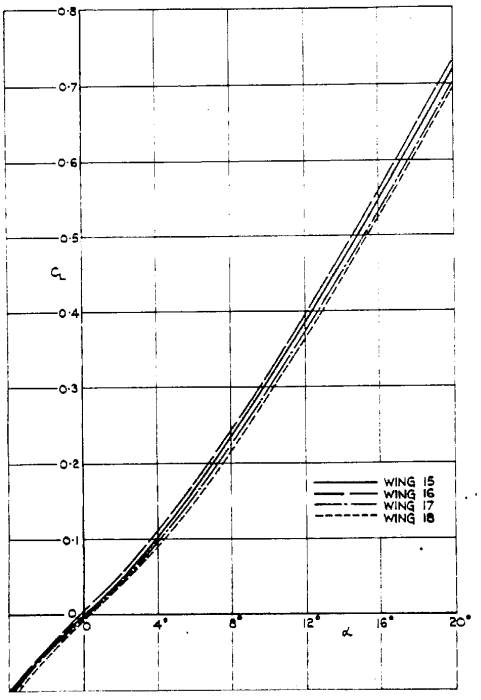

FIG. 11. Lift vs. incidence, $M \simeq 0{\cdot}3$.

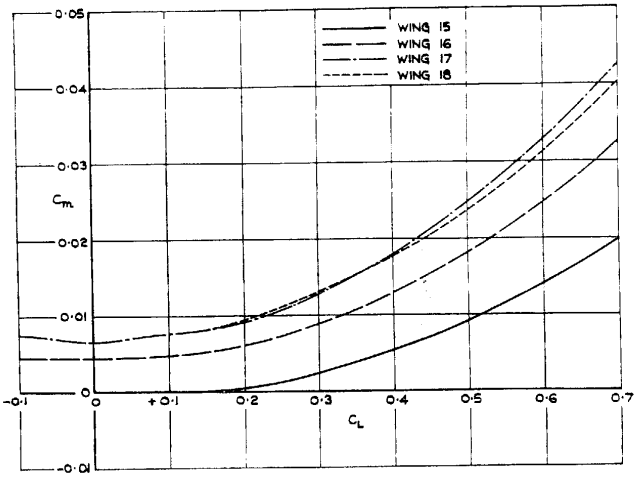

FIG. 12. Pitching moment vs. lift, $M \simeq 0{\cdot}3$.

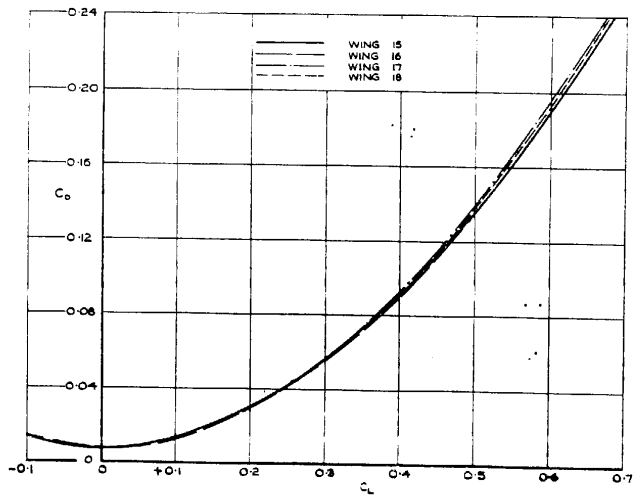

FIG. 13. Drag vs. lift, $M \simeq 0{\cdot}3$.

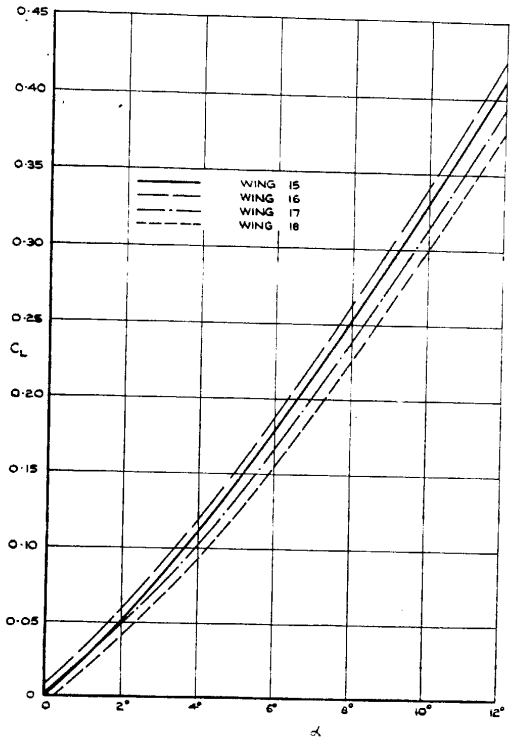

FIG. 14. Lift vs. incidence, $M \simeq 0{\cdot}8$.

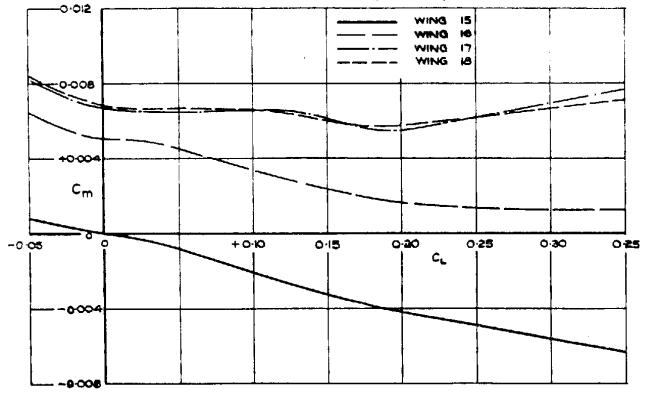

FIG. 15. Pitching moment vs. lift, $M \simeq 0{\cdot}8$.

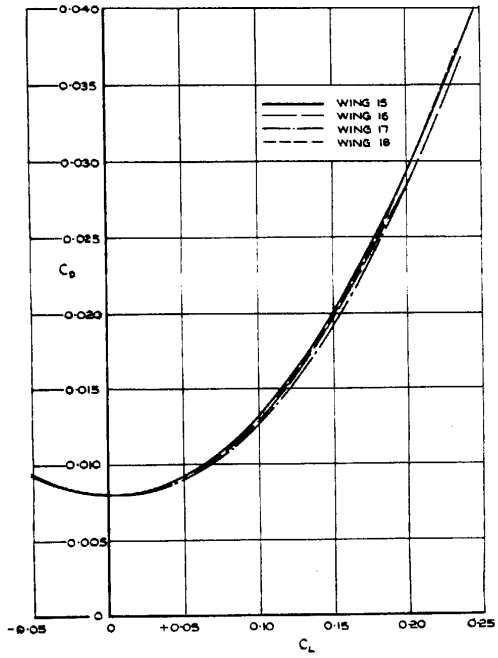

FIG. 16. Drag vs. lift, $M \simeq 0{\cdot}8$.

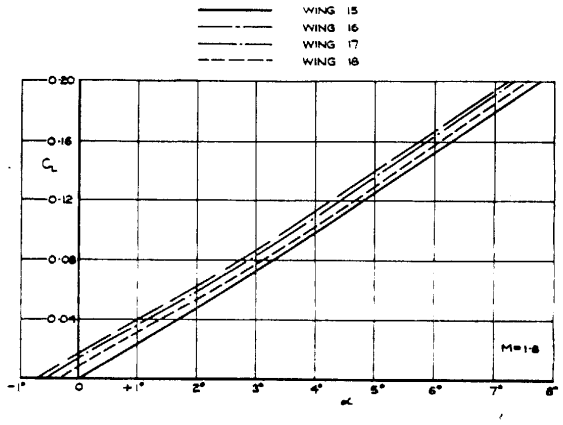

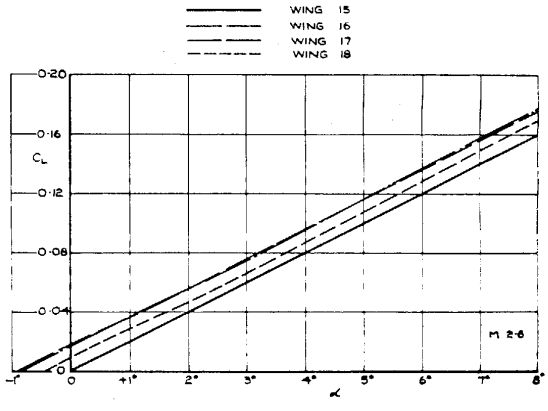

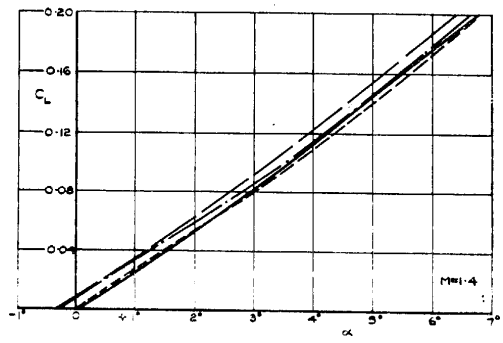

FIG. 17. Lift vs. incidence, $M = 1{\cdot}4$ and $1{\cdot}8$.

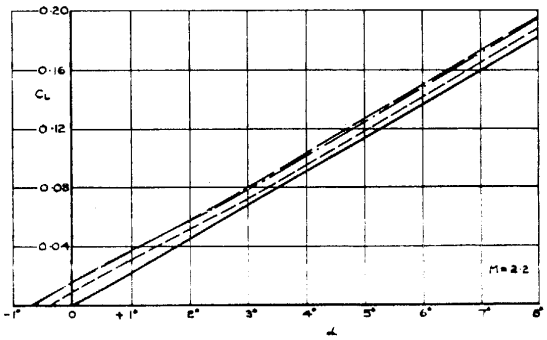

FIG. 18. Lift vs. incidence, $M = 2{\cdot}2$ and $2{\cdot}6$.

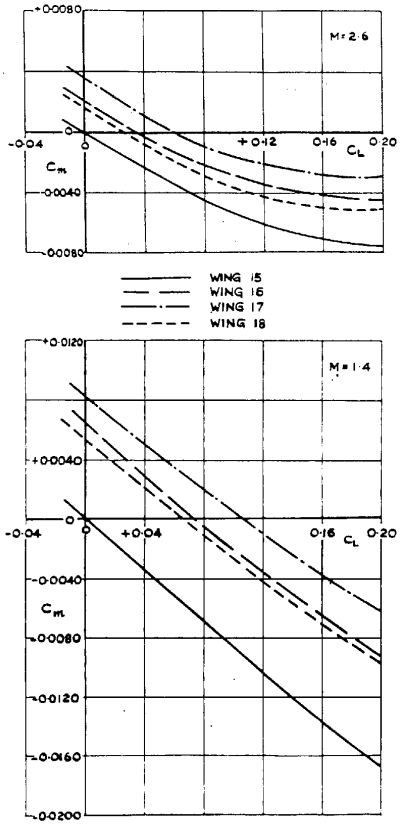

FIG. 19. Pitching moment vs. lift, M = 1·4 and 2·6.

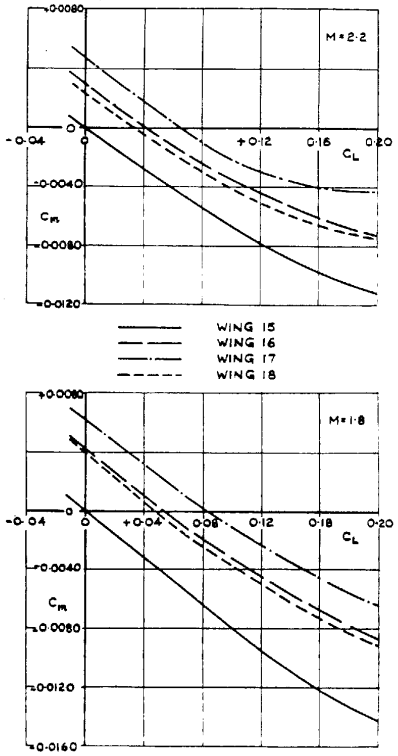

FIG. 20. Pitching moment vs. lift, M = 1·8 and 2·2.

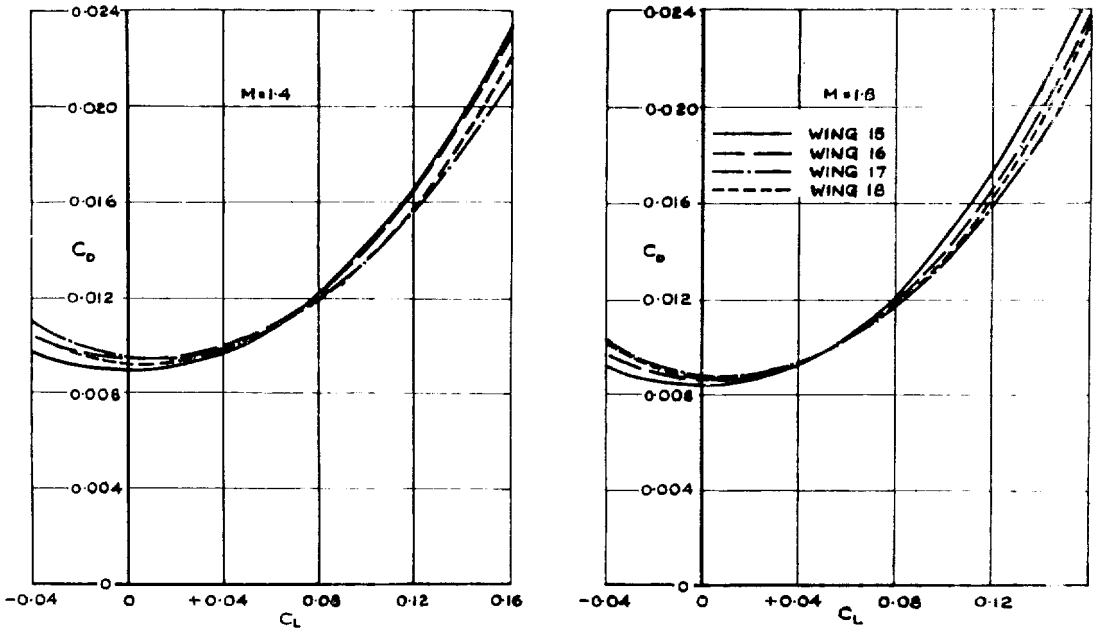

FIG. 21. Drag vs. lift, $M = 1{\cdot}4$ and $1{\cdot}8$.

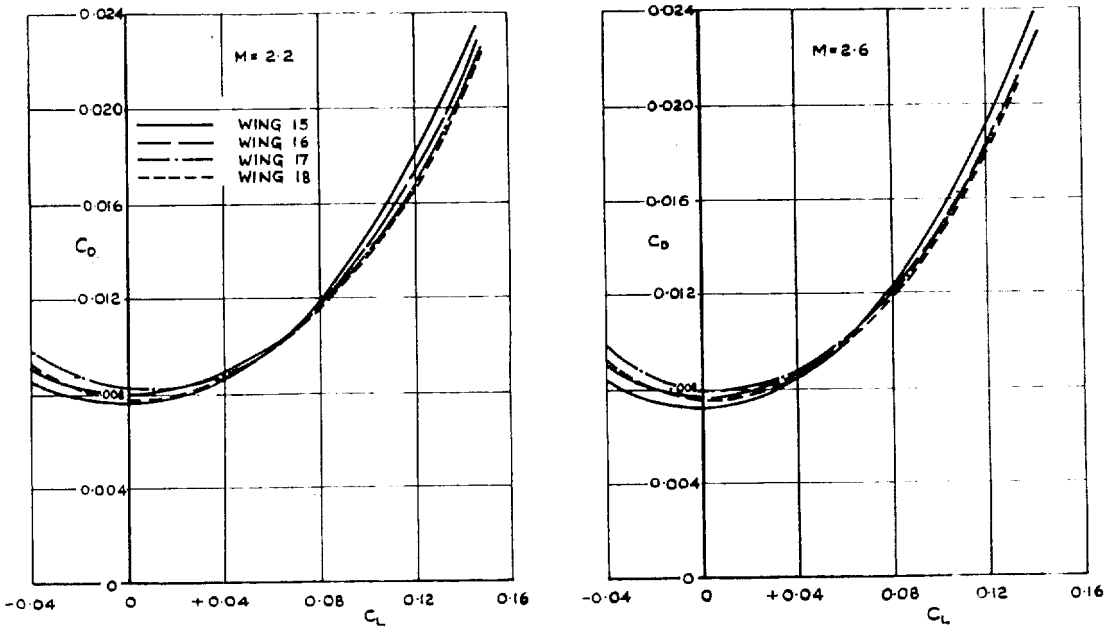

FIG. 22. Drag vs. lift, $M = 2{\cdot}2$ and $2{\cdot}6$.

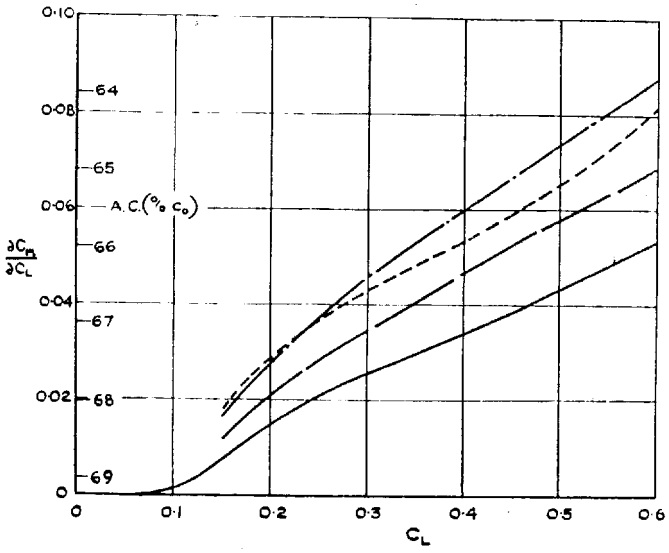

FIG. 23. Variation of aerodynamic-centre positions with lift coefficient, $M \simeq 0{\cdot}3$.

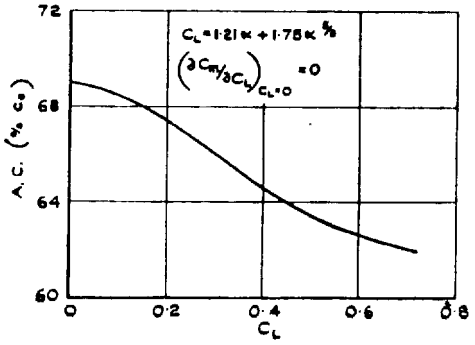

FIG. 24. Variation of aerodynamic centre of non-linear lift; wing 15, $M \simeq 0{\cdot}3$.

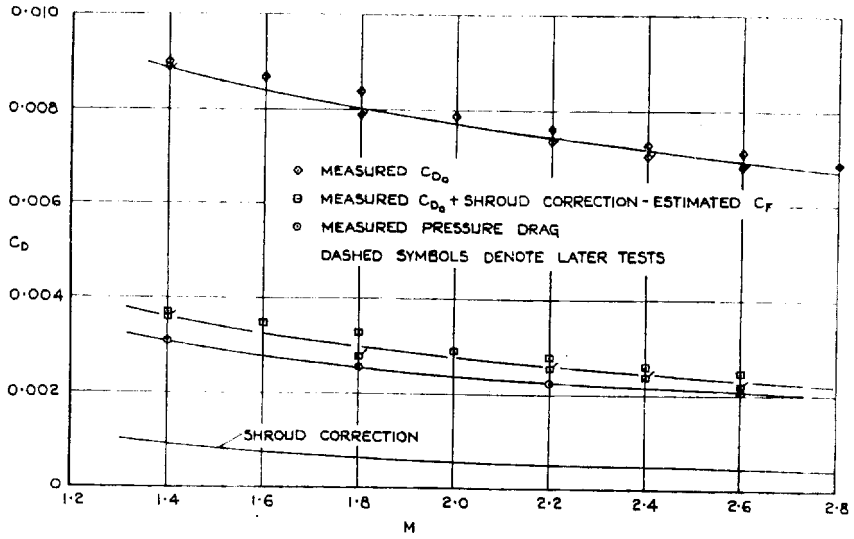

(a) $R = 10^7$.

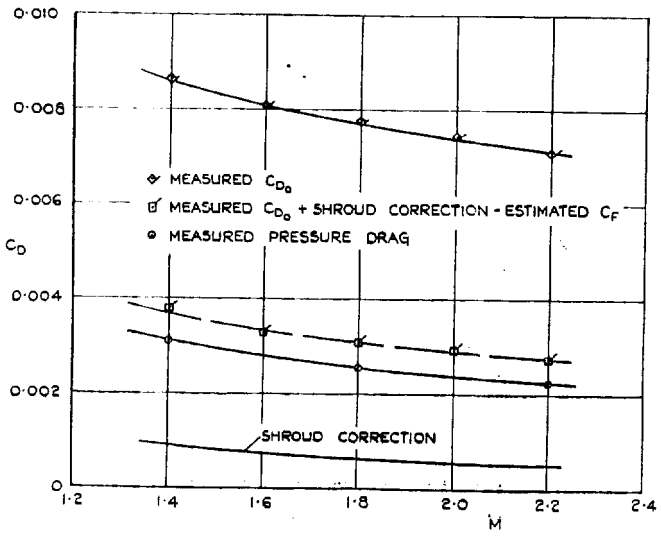

(b) $R = 1{\cdot}5 \times 10^7$ (later tests).

FIG. 25. Analysis of zero-lift drag of wing 15.

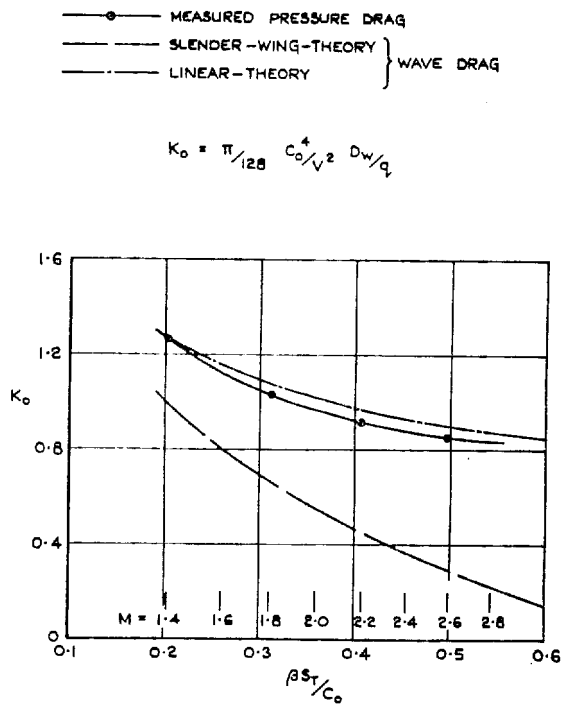

FIG. 26. Variation of K_0 with Mach number, wing 15.

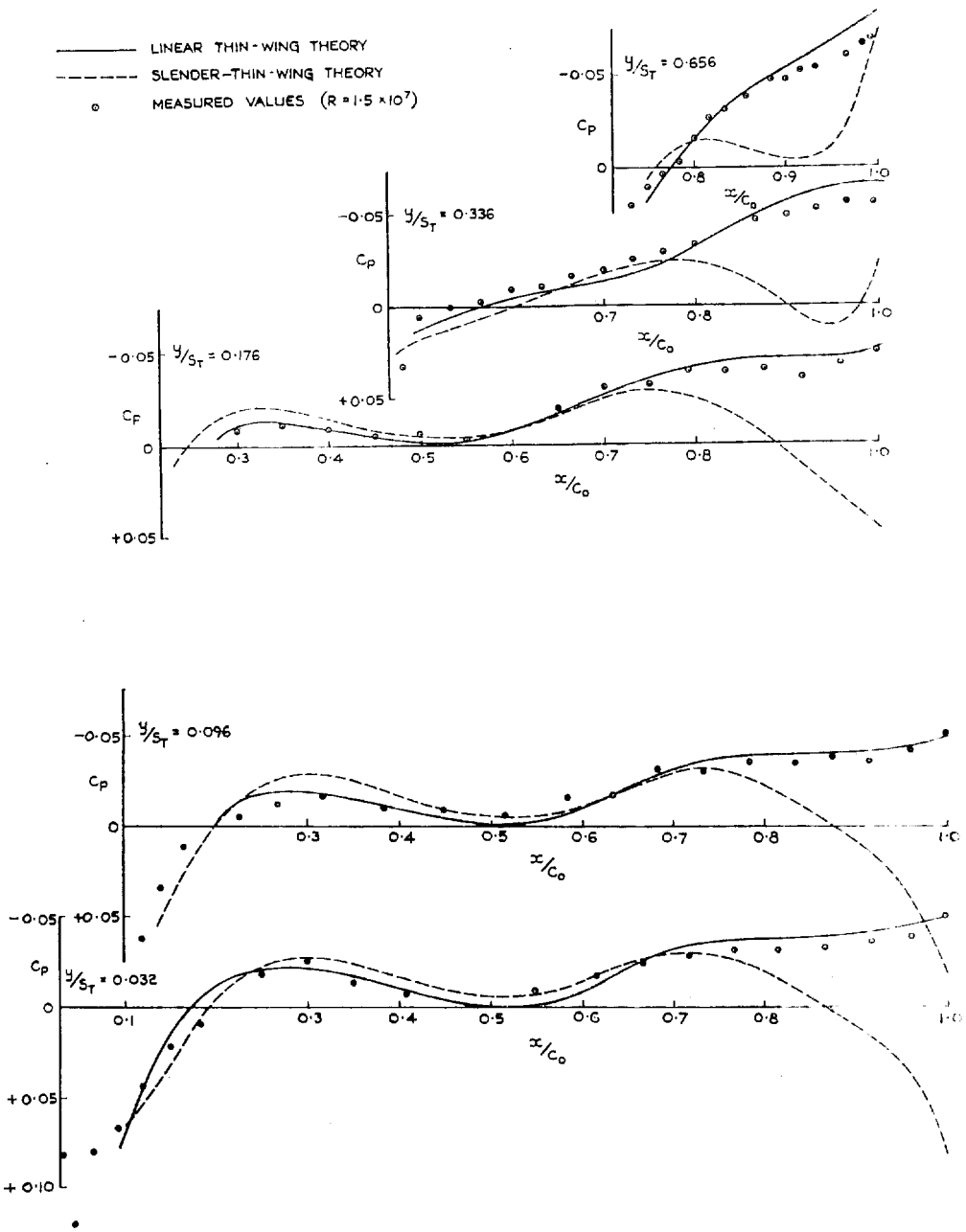

FIG. 27. Comparison of measured pressure distribution for wing 15, at $C_L = 0$, with two theoretical distributions. $M = 2{\cdot}2$.

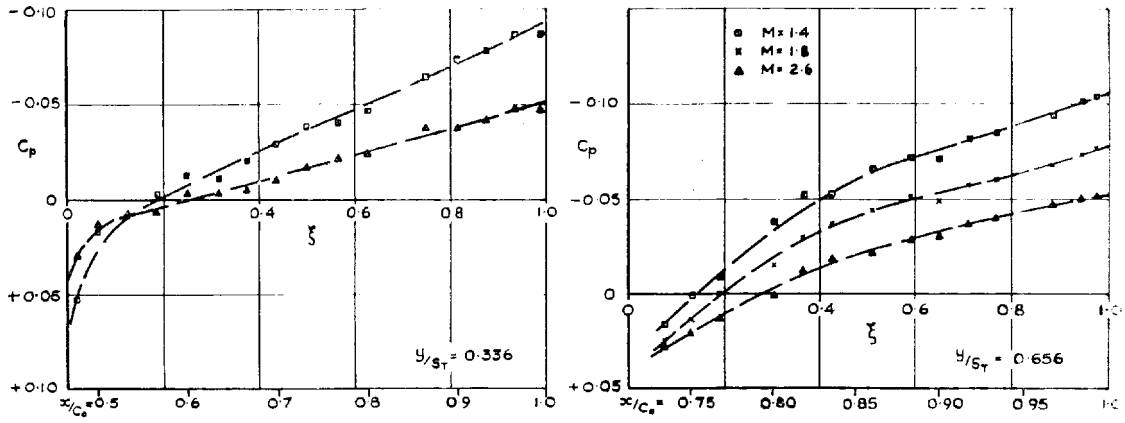

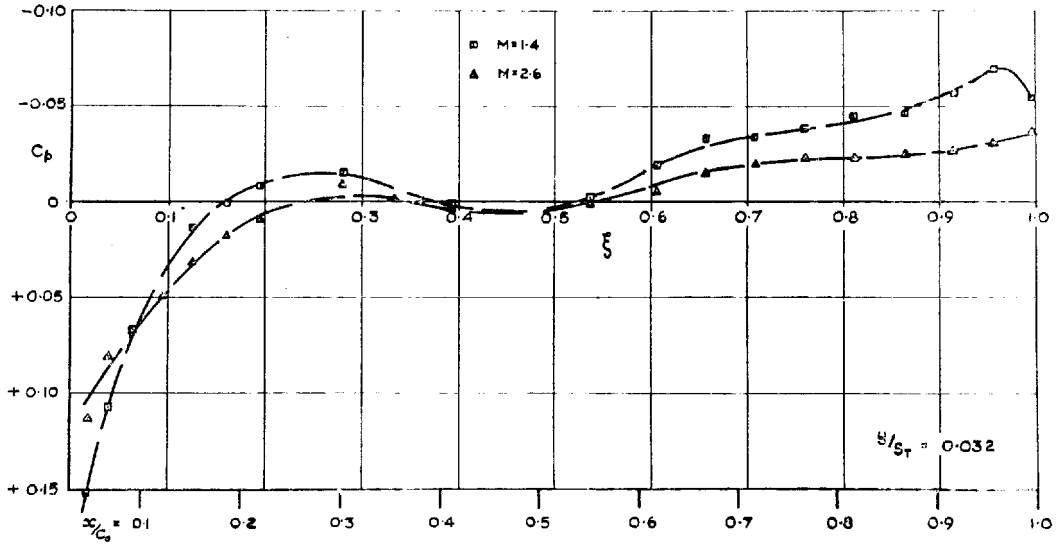

FIG. 28. Variation with Mach number of zero-lift pressure distribution for wing 15.

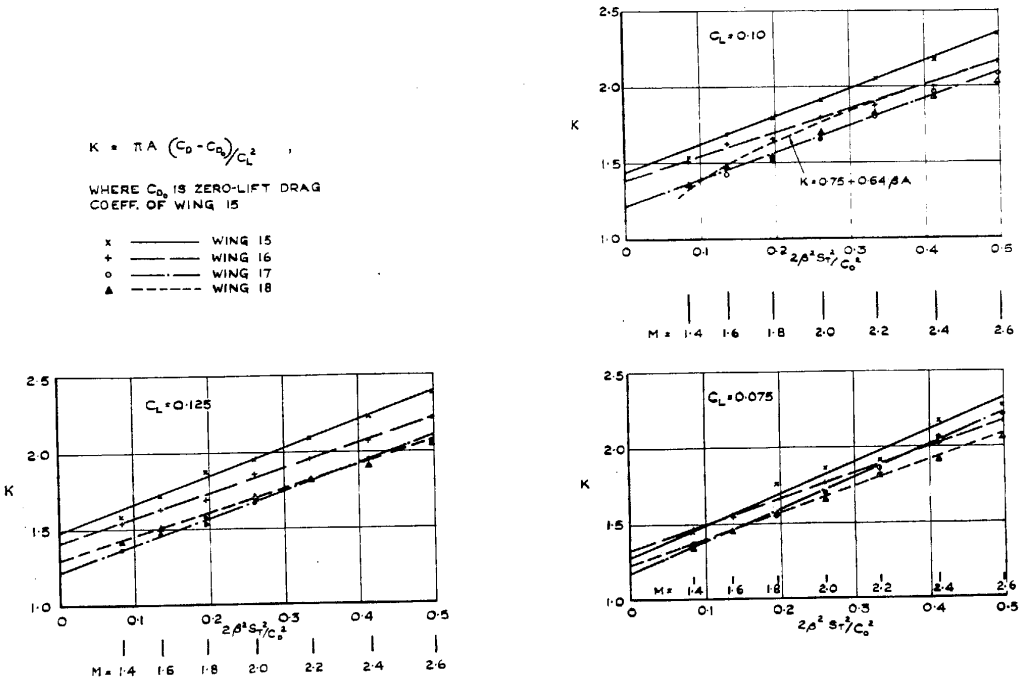

FIG. 29. Variation of drag-due-to-lift factors with Mach number.

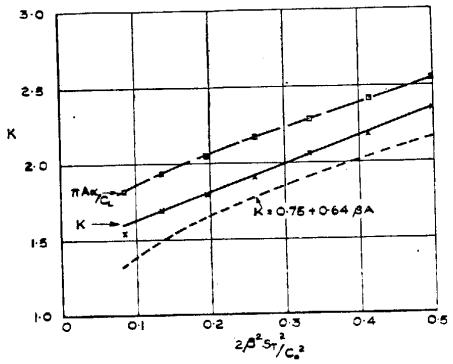

FIG. 30. Lift-dependent drag of the plane wing, $C_L = 0{\cdot}10$.

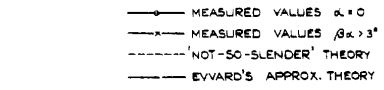

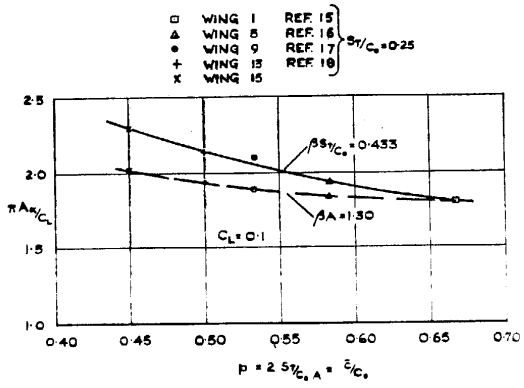

FIG. 31. Variation of $\pi AK/C_L$ with p for plane wings.

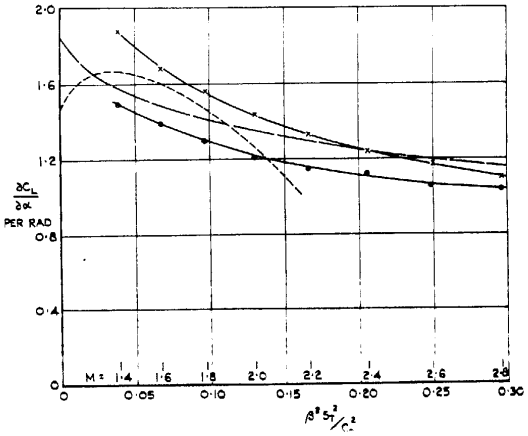

FIG. 32. Variation of $\partial C_L/\partial\alpha$ with Mach number, wing 15.

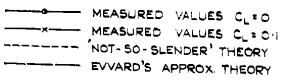

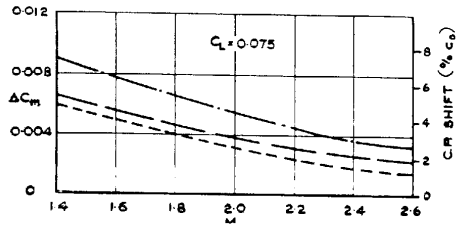

FIG. 34. Variation with Mach number of ΔC_m at constant C_L, wings 16 to 18.

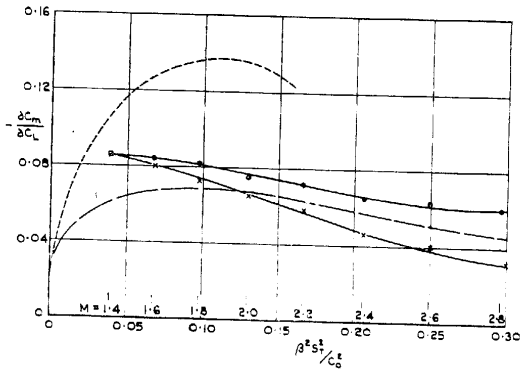

FIG. 33. Variation of $-\partial C_m/\partial C_L$ with Mach number, wing 15.

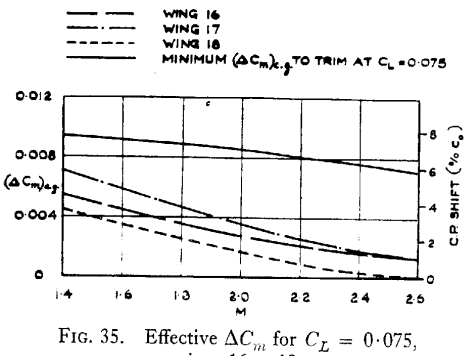

FIG. 35. Effective ΔC_m for $C_L = 0{\cdot}075$, wings 16 to 18.

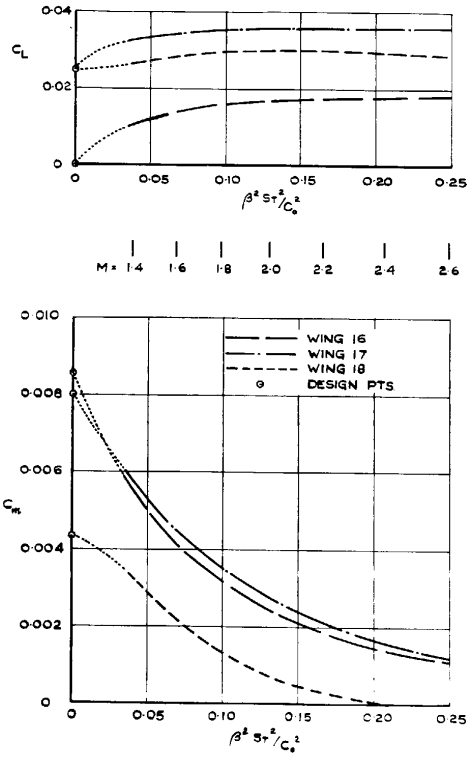

FIG. 36. Variation of C_L and C_m at design attitude with Mach number, wings 16, 17 and 18.

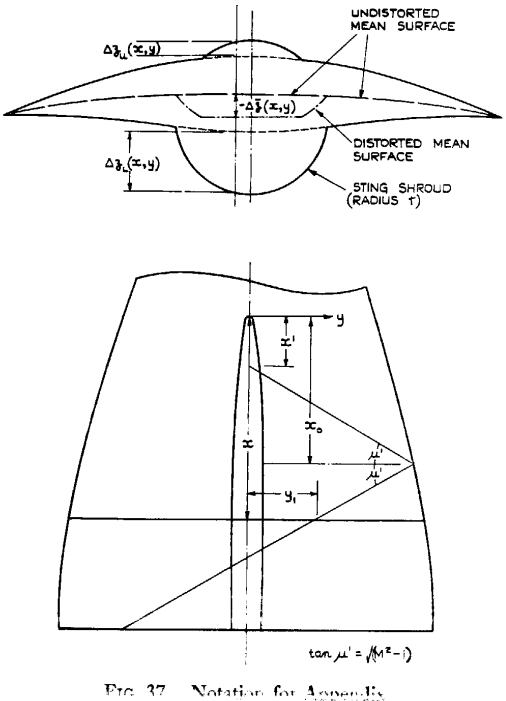

FIG. 37. Notation for Appendix

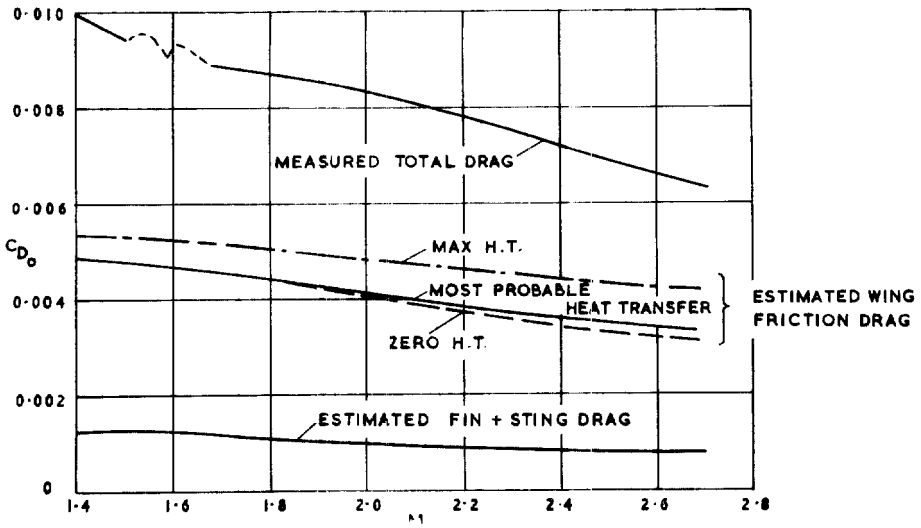

FIG. 38. Free-flight measurements of zero-lift drag of wing 15.

FIG. 39. Free-flight model.

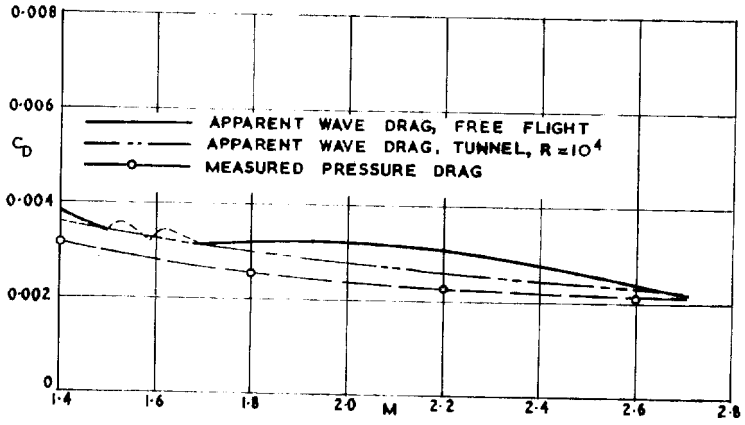

FIG. 40. Comparison of free-flight measurements with tunnel results.

(87542) Wt. 64/1857 K5 8/63 Hw.

Approved For Release 2002/10/16 : CIA-RDP71B00822R000100080002-8

A.R.C. R. & M. No. 3328 — 533.693.3:
December, 1961 — 533.6.011.34/.5:
C. R. Taylor — 533.6.013.12/.13:
533.6.013.15

MEASUREMENTS, AT MACH NUMBERS UP TO 2·8, OF THE LONGITUDINAL CHARACTERISTICS OF ONE PLANE AND THREE CAMBERED SLENDER 'OGEE' WINGS

Measurements have been made of the longitudinal characteristics of one plane and three cambered slender ogee wings ($p = 0 \cdot 45$, $s_T/c_0 = 0 \cdot 208$) at two subsonic and eight supersonic Mach numbers up to 2·8. The tests also included measurements of the zero-lift pressure drag and support interference of the plane wing. The results have been analysed to give data for estimating the performance of supersonic transport aircraft.

A.R.C. R. & M. No. 3328 — 533.693.3:
December, 1961 — 533.6.011.34/.5:
C. R. Taylor — 533.6.013.12/.13:
533.6.013.15

MEASUREMENTS, AT MACH NUMBERS UP TO 2·8, OF THE LONGITUDINAL CHARACTERISTICS OF ONE PLANE AND THREE CAMBERED SLENDER 'OGEE' WINGS

Measurements have been made of the longitudinal characteristics of one plane and three cambered slender ogee wings ($p = 0 \cdot 45$, $s_T/c_0 = 0 \cdot 208$) at two subsonic and eight supersonic Mach numbers up to 2·8. The tests also included measurements of the zero-lift pressure drag and support interference of the plane wing. The results have been analysed to give data for estimating the performance of supersonic transport aircraft.

A.R.C. R. & M. No. 3328 — 533.693.3:
December, 1961 — 533.6.011.34/.5:
C. R. Taylor — 533.6.013.12/.13:
533.6.013.15

MEASUREMENTS, AT MACH NUMBERS UP TO 2·8, OF THE LONGITUDINAL CHARACTERISTICS OF ONE PLANE AND THREE CAMBERED SLENDER 'OGEE' WINGS

Measurements have been made of the longitudinal characteristics of one plane and three cambered slender ogee wings ($p = 0 \cdot 45$, $s_T/c_0 = 0 \cdot 208$) at two subsonic and eight supersonic Mach numbers up to 2·8. The tests also included measurements of the zero-lift pressure drag and support interference of the plane wing. The results have been analysed to give data for estimating the performance of supersonic transport aircraft.

A.R.C. R. & M. No. 3328 — 533.693.3:
December, 1961 — 533.6.011.34/.5:
C. R. Taylor — 533.6.013.12/.13:
533.6.013.15

MEASUREMENTS, AT MACH NUMBERS UP TO 2·8, OF THE LONGITUDINAL CHARACTERISTICS OF ONE PLANE AND THREE CAMBERED SLENDER 'OGEE' WINGS

Measurements have been made of the longitudinal characteristics of one plane and three cambered slender ogee wings ($p = 0 \cdot 45$, $s_T/c_0 = 0 \cdot 208$) at two subsonic and eight supersonic Mach numbers up to 2·8. The tests also included measurements of the zero-lift pressure drag and support interference of the plane wing. The results have been analysed to give data for estimating the performance of supersonic transport aircraft.

Approved For Release 2002/10/16 : CIA-RDP71B00822R000100080002-8